

Radial growth decline in a tropical Andean treeline in Bolivia

Rose Oelkers^{1,2}, Laia Andreu-Hayles^{1,3,4}, Rosanne D'Arrigo¹, Hung T. T. Nguyen², Arturo Pacheco Solana^{2,5}, Milagros Rodriguez-Caton^{2,6}, M. Eugenia Ferrero^{6,11}, Ernesto Tejedor⁷, Alfredo F. Fuentes^{8,9}, Carla Maldonado^{8,9}, Daniel Ruiz-Carrascal¹⁰

¹Lamont-Doherty Earth Observatory of Columbia University, Palisades, NY 10964, USA

²Department of Earth Science and Environmental Change, University of Illinois Urbana-Champaign, Urbana, IL, USA

³Ecological and Forestry Applications Research Center (CREAF), Bellaterra, Spain

⁴Catalan Institution for Research and Advanced Studies (ICREA), Barcelona, Spain

⁵Department of Land, Environment, Agriculture and Forestry (TeSAF), University of Padua, 35020 Legnaro, Italy

⁶Instituto Argentino de Nivología, Glaciología y Cs. Ambientales (IANIGLA), CONICET Mendoza, Argentina

⁷Department of Geology, National Museum of Natural Sciences-Spanish National Research Council (MNCN-CSIC), Madrid, Spain

⁸Herbario Nacional de Bolivia, Instituto de Ecología, Carrera de Biología, Facultad de Ciencias Puras y Naturales, Universidad Mayor de San Andrés, La Paz, Bolivia

⁹Latin America Department, Science & Conservation Division, Missouri Botanical Garden, St. Louis, MO, USA

¹⁰Innovation and Technological Development Directorate, Universidad EAFIT, Medellín, Colombia

¹¹Laboratorio de Dendrocronología, Universidad Continental, Huancayo, Peru

Correspondence to: Rose Oelkers roelkers@ldeo.columbia.edu; reo19@illinois.edu; urco19@illinois.edu

Abstract. The ~~impacts~~ **impact** of rising temperatures ~~in on~~ tropical treeline ecosystems remains understudied. Here we report on a ~~remarkable decline in the radial growth history of~~ **remarkable decline in the radial growth history of** *Polylepis pepeii* BB.Simpson ~~trees growing in Madidi National Park, a~~ **trees growing in Madidi National Park, a** tropical ~~tree species that grows in a monospecific forest setting at the~~ **tree species that grows in a monospecific forest setting at the** elevational treeline in the Andes-Amazon ecotone of Bolivia. Using dendrochronological methods, we developed an annually ~~resolved tree-ring width chronology spanning from~~ **resolved tree-ring width chronology spanning from** 1850 to 2018 C.E. To our knowledge this is the longest ~~tree-ring record of annual tree growth (169/168 yrs) for this species.~~ **tree-ring record of annual tree growth (169/168 yrs) for this species.** ~~This-The standardized ring-width chronology revealed a significant (p=0.01) radial growth decline in P. pepeii after 1997; which was also observed in other high elevation Polylepis forests of tropical South America (> 17° S; 4600 m a.s.l.). Between the 1962-1963 growth ring (i.e. 1963-2018). From 1960-2015, P. pepeii RW was mostly regulated by prior year minimum temperature and mean precipitation variability during the wet season (~November-March). RW-climate correlations suggest the observed growth decline at this tropical treeline is likely due to temperature driven moisture stresses. Smaller ring-width was smaller ring-widths were associated with drier and warmer conditions in the forest during the previous wet season (~November-March), while wetter and cooler conditions led to enhanced growth in the following year. Between P. pepeii radial growth decline occurred at the same time a significant increase in minimum temperature and decrease in precipitation and diurnal temperatures was observed both locally and regionally across tropical South America between 1960-2015, minimum temperature significantly increased during the wet season, while precipitation decreased. These climate trends observed in our~~

Formatted: Border: Top: (No border), Bottom: (No border), Left: (No border), Right: (No border), Between : (No border)

Style Definition

Formatted: Width: 8.27"

Formatted: Font color: Text 1

Formatted: Line spacing: Multiple 1.83 li

Formatted: Font: 10 pt, Font color: Text 1, English (United States), Not Superscript/ Subscript

Formatted: Font color: Text 1

Formatted: Font color: Text 1, English (United States)

Formatted

Formatted

Formatted: Font color: Text 1

Formatted: Default Paragraph Font, Font color: Text 1, English (United States)

Formatted: Font color: Text 1

Formatted: Font color: Text 1

Formatted: Font color: Text 1

Formatted: Font color: Text 1

Formatted

Formatted: Border: Top: (No border), Bottom: (No border), Left: (No border), Right: (No border), Between : (No border)

36 ~~study region in the Madidi National Park at treeline~~ may indicate a reduction in moisture convergence and transport to ~~such~~
37 ~~higher elevations where our forest is located.~~ elevation settings in the Andes. If temperature ~~continues~~continue to rise at current
38 rates, one of the highest-elevation tree species on the globe, *P. pepei*, ~~could face severe consequences~~pepei, may continue to
39 decline leading to forest mortality and jeopardizing the survival of treeline ecosystems.

40 1 Introduction

41 South American treelines or ‘high montane’ forests refer to the upper range limit of tree growth within the Andes Mountains,
42 and are the longest, most biodiverse ecotone in the tropical latitudes (Körner, 2012; Young and León, 2006; Zelazowski et al.,
43 2023). Whether or not such tropical treelines will remain stable under global warming is a topic of great concern due to
44 increasing anthropogenic and climate-related pressures that threaten South American forest dynamics. In recent decades, land-
45 use change and warming temperatures have led to observed shifts in species composition, distribution and increased tree
46 mortality in the tropical Andes treelines (Cuesta et al., 2020; Feeley et al., 2012, 2011; Macek et al., 2009; Young and León,
47 2006). In southern Peru, ice core records indicated that recent surface warming in the central Andes has been unprecedented
48 in the past 5000 years, and land-atmosphere models suggest the net primary production of upper montane forests in South
49 America will decrease as temperatures increase (Fajardo et al., 2019; Nagy et al., 2023; Thompson et al., 2006). Despite the
50 value of these modeling and plot-based studies of tropical South American treelines, our knowledge of forest age, annual
51 growth patterns, and historical response to climate trends remains limited.

52
53 Dendrochronological studies in tropical South America are generally scarce (~8°N-24°S) but have been key in reconstructing
54 long-term tree-growth and climate variability in the Andes (Andreu-Hayles et al., 2023; Groenendijk et al., 2025; Quesada-
55 Román et al., 2022). The stability of tropical Andean treeline communities under global warming has become of great concern
56 due to observed shifts in forest composition, distribution and increased tree mortality in recent decades (Cuesta et al., Trec-
57 ring studies have reported that several Andean treeline species form annual growth rings and that the width of the rings (i.e.
58 RW) are sensitive to precipitation and/or 2020; Feeley et al., 2012, 2011; Macek et al., 2009; Young and León, 2006). In South
59 America, forests found near the mountain peaks in the Andes Mountains are often referred to as ‘treeline’ or high mountain
60 areas in literature (Hoek et al., 2019; Körner, 2012; Young and León, 2006) and the term used herein is used to describe the
61 upper range limits of the tree species found in the region. Plot studies in the Peruvian Andes-Amazon found that the position
62 of Andean timberline (i.e. elevational limit of closed canopy forests) is limited by seed dispersal (Rehm and Feeley, 2013).
63 Dendrochronology has been widely used to evaluate annual growth variability and long-term climate response of treeline
64 forests in the northern Hemisphere (Büntgen et al., 2022; D’Arrigo et al., 1999; MacDonald et al., 2007). However, tropical
65 tree-ring studies in South America (~8°N-24°S), are noticeably scarce in comparison to higher latitude regions (Andreu-Hayles
66 et al., 2023; Groenendijk et al., 2025; Quesada-Román et al., 2022). Still, some relevant studies have provided key
67 understanding of climate-growth response of high elevation forests in the tropical Andes as described below:

Formatted: Border: Top: (No border), Bottom: (No border), Left: (No border), Right: (No border), Between: (No border)

Formatted: Font color: Text 1

Formatted: Font color: Text 1

Formatted: Font color: Text 1

Formatted: Font color: Text 1

Formatted: Border: Top: (No border), Bottom: (No border), Left: (No border), Right: (No border), Between: (No border)

68
69 A study from the Peruvian puna (upper Andes) presented the first tree-ring chronology of *Escallonia myrtilloides* L. Phil.
70 (Requena-Rojas et al., 2021), a species often found at tropical treeline (Zapata, 2013), in which the authors showed radial
71 growth is positively correlated to precipitation, and negatively correlated to temperature variability in this region. In the central
72 Andes of Peru, Requena-Rojas et al. (2020) analyzed the tree rings from three *Polylepis* species, and found these trees are
73 slow-growing and sensitive to both current-year temperature and prior-year precipitation changes. In subtropical regions, prior-
74 year moisture availability was the dominant limiting factor for e.g. *Escallonia myrtilloides*, *Polylepis tarapacana* Phil. treelines
75 in Argentina, based on RW-climate correlations spanning 1934-1980 (, *Polylepis reticulata* (Alvites et al., 2019; Argollo et
76 al., 2004; Morales et al. 2004) On the other hand, the growth of several tropical montane species in northern Argentina appears
77 to be regulated only by temperature at the upper elevations of an altitudinal gradient (Ferrero et al., 2013). Although seedling
78 recruitment of *Nothofagus pomillo* is driven by temperature (, 2004; Requena-Rojas et al., 2021, 2020). The relationship
79 between annual RW in treeline species and local climate variability, the rate of seedling establishment was limited by overall
80 moisture conditions in Patagonia (Srur et al., 2018, 2016). Yet, there was a radial-growth decline in *Nothofagus pumilio* at a
81 Chilean treeline site, where precipitation had increased (Álvarez et al., 2015), possibly suggesting a non-linear growth response
82 of these forests to climate.

83
84 Here we describe a tropical treeline site of in the tropics can vary depending on the latitudinal and elevational position of the
85 forest along the Andes (e.g. *Polylepis peppei* BB.Simpson (Simpson, 1979), growing high elevations (3800–4000 m.a.s.l.) in
86 the Andes-Amazon corridor of Bolivia in South America. This site is located at upper forested limit of Bolivia's Madidi
87 National Park (MNP), a hotspot for biodiversity just east of the Cordillera Real in the Andes. Temperature and humidity
88 gradients shape unique ecotones in the MNP including diverse seasonally dry forests near the Tuichi River (~850 m.a.s.l.) and
89 humid monospecific forests at Andean treeline (~4400 m.a.s.l.). The hydroclimate of the MNP (and Andes-Amazon) is
90 primarily in northern vs. Southern Bolivia (Jomelli et al., 2012; Roig et al., 2001). Hydroclimate conditions in South America
91 are largely influenced by the South American Summer Monsoon (SASM), which peaks in the tropics during austral summer
92 (December-February). Inter-annual to decadal sea surface temperature (SST) conditions in the Pacific
93 and Atlantic Oceans also impact climate in the region (Paegle and Mo, 2002; Vuille et al., 2000). Originating in the tropical
94 Pacific, the El Niño–Southern Oscillation (ENSO) system is the dominant mode of annual to decadal hydroclimate variability
95 in South America and indeed the globe (e.g.,). In addition to inter-annual and decadal fluctuations in temperature and
96 precipitation, circulation patterns related to the timing and strength of the South American Summer monsoon, are modulated
97 by ENSO as well (Garreaud, 2009; Vera et al., 2006; Vuille et al., 2000). ENSO-related anomalies SST anomalies have
98 contributed to extreme weather events in South America such as seasonal drought, flooding, and other geohazards (Vera et al.,
99 2006; Vuille et al., 2000). Free At the central tropical Andes treeline, *Polylepis tarapacana* tree-ring width (RW) and oxygen
100 isotopes have recorded these extreme events at treeline *P. tarapacana* in the central tropical Andes and provided year-
101 to-year to centennial records of ENSO variability overall (Christie et al., 2009; Crispin-DelaCruz et al., 2022; Rodriguez-Caton

Formatted: Border: Top: (No border), Bottom: (No border),
Left: (No border), Right: (No border), Between : (No border)

Formatted: Border: Top: (No border), Bottom: (No border),
Left: (No border), Right: (No border), Between : (No border)

102 et al., 2022) Currently there is no information on the impacts of such ENSO-related climate extremes on *Polylepis pepeii* tree-
103 rings, or for treeline sites within the MNP.

104
105 *Polylepis* is the dominant genus for tropical Andes treelines and represent the highest elevation tree species in South America
106 (Pyre et al. 2025; Simpson 1979). The name *Polylepis* is derived from the Greek word ‘many layers’, which refers to the
107 multiple sheets of thin, compressed bark useful for thermal insulation at high elevations (Rada et al. 2001; Rodriguez-et al.
108 2021). However, as the climate warms, frost tolerance may no longer be an advantageous trait, and some studies predict that the
109 germination and spatial distribution of *Polylepis* at the treeline will decrease as vapor pressure deficits, temperatures, and
110 overall aridity increase in the Andes (Cuyckens et al., 2016; López et al., 2022). The geographic range of *Polylepis* To date, it
111 is not known whether such projected decline has already occurred in treeline *Polylepis* populations.

112
113 Here we describe a new tree-ring record of *Polylepis pepeii* from a treeline site at the Madidi National Park (MNP) in Bolivia,
114 a hotspot for biodiversity in the southwestern Andes-Amazon region in Bolivia (BB.Simpson)(Simpson, 1979). The
115 geographic range of *P. pepeii* (family Rosaceae; common name “Kenua” or “Queñoa”) spans from central Bolivia to northern
116 Peru (Simpson, 1979) between 3550-4800 m.a.s.l. (Espinoza and Kessler, 2022). The wide dispersion of leaves and long fruit
117 distinguishes *P. pepeii* from other *Polylepis* species. Tree-ring studies in Bolivian and Peru have shown *P. pepeii* can reach
118 significant age (>135 years) and the RWring-width can be sensitive to both prior and current-year climate variability (Jomelli
119 et al., 2012; Roig et al., 2001). The wide dispersion of leaves along the branches in *P. pepeii* and its long fruit distinguish this
120 species from other *Polylepis* spp. The genus name *Polylepis* is derived from the Greek words ‘many layers’, describing
121 multiple layers of compressed thin bark sheets, a functional trait that allows these trees to survive freezing air temperatures.
122 This species is also adapted to cold soil temperatures in the eastern cordillera of the Andes. Ecological studies of *P. pepeii* sites
123 between 3800-4300 m.a.s.l. in Peru (Kessler et al., 2014) and Bolivia (Hoch and Körner, 2005) recorded (>5cm)shallow soil
124 temperatures ranging from 3-5°C during the wet season-

125
126 (Kessler et al. 2014; Hoch and Körner, 2005). Like much of the treeline species across the Andes-Amazon, *P. pepeii* is under
127 threat of shifting temperature regimes and human impacts on the ecosystem. Some studies predict the germination and spatial
128 distribution of treeline *Polylepis* spp in the Andes is projected to decrease as vapor pressure deficits, temperatures, and overall
129 aridity increase (Cuyckens et al.,

130
131 In the small community of Keara Bolivia where this study is located, 2016; López et al., 2022). Southwest of our *P. pepeii* site,
132 in the central Andes of southern Peru ice proxy data indicated recent surface warming in the tropics that appears unprecedented
133 in 5000 years (Thompson et al., 2006). In November 2009, temperatures were so warm that a catastrophic glacial lake outburst
134 flood eliminated roads, livestock, and structures in the small community of Keara Bolivia (<November 2009 (~3800 m.a.s.l.;
135 Hoffmann and Weggenmann, 2013). In the MNP, there is evidence of a temperature induced A recent forest-monitoring study

Formatted: Border: Top: (No border), Bottom: (No border),
Left: (No border), Right: (No border), Between : (No border)

Formatted: Font color: Text 1

Formatted: Font color: Text 1

Formatted: Font color: Text 1

Formatted: Font color: Text 1

Formatted: Border: Top: (No border), Bottom: (No border),
Left: (No border), Right: (No border), Between : (No border)

136 ~~in the MNP observed an upslope migration (i.e. thermophilization) of mid-elevation tree species towards Andes ecotones~~
137 ~~caused by due to increased of temperatures and tree mortality nearin the treelineUpper Andes vegetation~~ (Farfan-Rios et al.
138 2025).

139
140 ~~Humans also play a role in modifying the forested landscape near the MNP. Illegal mining and logging activities in low~~
141 ~~elevation forests (<1200 m.a.s.l.) have deteriorated forest structure and health, with increasing loss of forest cover in recent~~
142 ~~years (Finer and Mamani, 2023). Prior to the designation of Madidi as a National Park in 1995, large swaths of economically-~~
143 ~~valuable trees along riverbanks (e.g. *Amburana cearensis* Smith) were harvested for timber (e.g. *Amburana cearensis*; Macía,~~
144 ~~2008). TodayIn recent years, illegal mining and logging activities have deteriorated forest structure and health, with increasing~~
145 ~~loss of forest cover at lower-elevations (below 2000 m.a.s.l; Finer and Mamani, 2023). At treeline, *P. pepei* is at great risk of~~
146 ~~endangerment due to habitat loss related to fires and land conversion for cattle ranching or religious practices (Espinoza and~~
147 ~~Kessler, 2022; Kessler et al., 2014). These losses of primary forests have severe implications for carbon storage capacity,~~
148 ~~ecosystem function, and land stability, all critical factors for the survival of native inhabitants. Herein, efforts were made to~~
149 ~~minimize potential impacts of land use and disturbance in field sampling, but ecosystem disturbances in certain regions of the~~
150 ~~MNP were nevertheless observed. Since this ecotoneSince the MNP~~ is facing a rapidly changing environment due to climate
151 and human-related disturbances, high resolution tree-ring records ~~at this treeline~~ may offer valuable insight on the past and
152 current growth responses.

153
154 response of this treeline to rising temperatures. At present, only two tree-ring studies have been published for the MNP: one
155 for *Juglans boliviana* (C.DC.) ~~Dodein Oelkers et al. (2023)~~ (14°40' S, 68°41' W; 1300 m.a.s.l.) ~~in Oelkers et al. (2023)~~ and
156 another by *Andreu-Hayles et al. (2015)*, the latter confirming the formation of annual rings in a *Pseudomedia rigida* (Klotzsch
157 & H.Karst.) ~~Cuatree~~ cross-section (14°33'S, 68°49'W; 1000 m.a.s.l). The *Polylepis pepei* ~~site investigatedobjectives~~ for this
158 study ~~is found between ~3800-4400 m.a.s.l. in the western MNP (14°40' 14°43'S; 69°04' 69°06'W)~~. Located near the small
159 settlement of Keara, the vegetation is characterized as Alto Andino Yungueño (Upper Andean Yungas) forest (Navarro et al.,
160 2010) with a seasonally humid climate. This study area was chosen in part because inventory plots already exist at this location,
161 established by botanists from the National Herbarium in La Paz (Bolivia) and the Missouri Botanical Garden (USA). Our
162 specific objective are: i.) to generate a newthe first RW chronology for *P. pepei-pepei* in the MNP and assess radial growth
163 patterns; ii.) to identify the primary climate variables (e.g. mean-temperature, or precipitation, drought), that are the most
164 limiting for annual) modulating tree growth variability, and iii.) to assess the impacts of extreme climate events on the RW
165 variations. at this treeline.

Formatted: Border: Top: (No border), Bottom: (No border),
Left: (No border), Right: (No border), Between : (No border)

Formatted: Border: Top: (No border), Bottom: (No border),
Left: (No border), Right: (No border), Between : (No border)

2 Materials and Methods

2.1 Site description and climatology

2.1.1 Climate data

The network of *Polylepis pepeii* for this study site is located in northwestern Bolivia (Fig. 1A), where two locations were visited in October 2012 and July 2019 to extract samples of *P. pepeii* trees at altitudinal treeline in Keara (Fig. 1C, D). Two to four core samples were extracted from living trees using 2-threaded increment borers (5 mm in diameter). Cross sections of recently dead trees were sliced using a gas-powered chainsaw or a standard saw-tooth blade. In 2019, diameter at breast height (DBH; ~1.2 m) was measured for the trees at the same level that core samples were extracted.

The 2012 collection was from an open canopy south-facing forest (the MNP near the small community of Keara, Bolivia (14°42'S, 69°05'W; 3795–4100 m.a.s.l.), while the 2019 collection was primarily focused in a closed canopy west-facing stand in a high elevation valley called Waca-cocha (named after a nearby lagoon; 4000–4400 m.a.s.l.; Fig. 1D). Both sites feature seasonally humid, upper-montane forests, with persistent mist that evaporates during the day. The sites were largely monospecific, dominated by fragmented patches of *P. pepeii* and small numbers of *Gynoxys compressissima* Cuatrec. trees. Based on field observations in July 2019, the foliage of *P. pepeii* may be considered evergreen and the bark consists of thick layers of compressed flakes that are red and brown in color, characteristic of the genus (Appendix A: Fig. A2A). The trees are shrublike, with twisted (and at times, multiple) stems.

The climatology of the study site (1960–2015 Figs. 1B, A1) shows a distinct wet season from October–April and a dry season from June–August (1960–2015; Fig. 1B). The wet season is defined by heavy rainfall (~1900 mm in January; Pre), and warmer mean (6° ; Tavg) and maximum temperatures (Tmax; 12–14.7°C). In contrast, the dry season is characterized by low precipitation (65 to 115 mm per month) and extremely cold temperatures (minimum temperature range 7.1 to 8.3°C; Fig. A1). Consistent with these patterns the mean diurnal temperature range (the difference between Tmax and Tmin, DTR; Fig. A1–B) is smallest during the peak wet season (12.1 to 16.9°C) due to warmer minimum temperatures (-0° C), and highest during the drier months. Wet season precipitation and temperature (Oct–Apr) was significantly and negatively correlated between 1960–2015 ($r=-0.27$, $p=0.05$) indicating wetter months at this site are typically associated with cooler temperatures, while no significant correlations were found during the dry season.

2.2 Climate data

In this study, we used local precipitation data, and gridded temperature products were used to generate monthly climate indices near Keara (1960–2015; Fig. 1B) for the site between 1960 and 2015. This period was selected for the site climatology and climate-growth analyses due to the limited availability of continuous precipitation data for this region of Bolivia. Daily precipitation from the Italaque station in Bolivia (15.48°S, 69.03°W; 3500 m.a.s.l.) was gap filled and homogenized with

Formatted: Border: Top: (No border), Bottom: (No border), Left: (No border), Right: (No border), Between : (No border)

Formatted: Font color: Text 1

Formatted: Font color: Text 1

Formatted: Font color: Text 1

Formatted: Font color: Text 1

Formatted: Border: Top: (No border), Bottom: (No border), Left: (No border), Right: (No border), Between : (No border)

199 ~~nearby station data~~ to generate a continuous monthly timeseries ~~(Pre) from 1960-2015 following procedures described in~~
200 ~~Huerta et al. (2025a) and using the 'redprecc' package in R (Huerta et al. 2025b). Raw (daily, 2026). Nearest-neighbor~~
201 ~~interpolation was constrained to precipitation stations above 3000 m.a.s.l. Raw~~ precipitation data for Italaque (1978-2005) and
202 nearby stations (~1945-2015, non-continuous) ~~ean-bewere~~ obtained from the DECADE dataset ~~(Hunziker et al. 2018)~~, which
203 were originally sourced from the National Meteorology and Hydrology Service of Bolivia ~~(Hunziker et al., 2018)~~(SENAMHI;
204 ~~https://senamhi.gob.bo/index.phphttps://senamhi.gob.bo/index.php~~). ~~Monthly mean (Tavg), minimum (Tmin), maximum~~
205 ~~(Tmax) temperature data was obtained from the Climatic research Unit TS 4.08 (CRU; 0.5° resolution; Harris et al. 2020). In~~
206 ~~addition, we also used CRU monthly diurnal temperature range (DTR; 0.5° resolution; 1901-2015), which represents the~~
207 ~~difference between Tmax and Tmin, to evaluate temperature variability in the region. The monthly climatology (1960-2015)~~
208 ~~and long-term variability of DTR (and Tmax and Tmin; 1901-2015) can be found in Appendix A Figs. A1 and A4 (see section~~
209 ~~2.5 for more details). Satellite-derived rainfall data from the Climate Hazards Infrared Precipitation with Station group V2.0~~
210 ~~(CHIRPS, accessed 2025; (Funk et al., 2015))~~ was used for spatial precipitation analyses (see Section 2.5-6). ~~Precipitation~~
211 ~~and temperature from the Climatic research Unit TS 4.08 was used to determine the average climate during years of known~~
212 ~~ENSO-DJF events between 1901-2018 (see section 2.7; nearest grid point 14.75°S, 69.25°W;(Harris et al., 2020)).~~
213 ~~Precipitation values from the nearby station were also evaluated for climate during extreme ENSO years, but the timeseries is~~
214 ~~limited to the period of 1960-2015.~~ Although CHIRPS v2.0 is limited to observations after 1981, it has a higher spatial
215 resolution (0.05°) than ~~CRU~~Climatic research Unit TS 4.08 precipitation (0.5°), which can be more effective for spatial
216 climate-growth analyses in regions with complex topography such as our site in the Andes-Amazon.

217
218 ~~Monthly mean, minimum, maximum temperature data (Tavg, Tmin, Tmax) from the nearest CRU grid point were used for~~
219 ~~local temperature-growth analyses (1960-2015; 14.75°S, 69.25°W). CRU minimum and maximum temperatures for tropical~~
220 ~~south America region (15°N~24°S, 82°W~39°W) were used for spatial correlation analyses with the *Polylepis pepei* ring-~~
221 ~~width chronology (see section 2.6 for more details). In addition to the 1960-2015 climate-growth analysis period, we also used~~
222 ~~CRU monthly diurnal temperature range (i.e. DTR; the difference between Tmax and Tmin) to evaluate long-term annual~~
223 ~~temperature variability at the site between 1901-2015, as well as seasonally for the wet (October to April) and dry (June to~~
224 ~~August) seasons.~~

225
226 ~~In situ high-resolution climate data was also obtained for this study. In August 2011 (one year before the 2012 sampling~~
227 ~~campaign), HOBO@® temperature and relative humidity data loggers (<https://www.onsetcomp.com/>) were installed near the~~
228 ~~*P. pepei* trees at (14°40'S, 69°06'W (-4158 m.a.s.l.) and data was recorded hourly from 1 September 2011 to 2 September~~
229 ~~2014. New HOBO sensors were installed in 2021 and collected during fieldwork in 2023. Unfortunately, the 2021 system~~
230 ~~batteries failed within 9 months of the launch, and data was limited to only 20 September 2021 to 23 May 2022. Daily To~~
231 ~~compare the in-situ records of wet-season climate with the long-term DTR data, daily~~ minimum, maximum and mean
232 temperature and relative humidity ~~were~~was calculated from ~~20 September 1 October to 23 May (24530 April (~212 days) for~~

Formatted: Border: Top: (No border), Bottom: (No border), Left: (No border), Right: (No border), Between : (No border)

Formatted: Font color: Text 1

Formatted: Font color: Text 1

Formatted: Border: Top: (No border), Bottom: (No border), Left: (No border), Right: (No border), Between : (No border)

233 the 2011-2012, 2012- 2013, 2013-2014 and 2021-2022 periods (see Appendix A Fig. A3. Kernel density estimates were used
234 to generate and compare probability seasons. Daily climate distributions were visualized using ridgeline density curves
235 generated with the 'ggridges' package in R (Wilke and Wilke, 2022). Differences among the daily time series.
236 Nonparametric four seasonal distributions for temperature and humidity were evaluated using the nonparametric Kolmogorov-
237 Smirnov (KS) test statistic and implemented via the 'stats' package in R (Kolmogorov, 1933; Smirnov, 1948) were conducted
238 to determine the significance of the mean difference between the). To account for serial dependence in daily timeseries. Kernel
239 density and KS tests were conducted using seaborn (Waskom, 2021) and SciPy (Virtanen et al., 2020) packages in
240 python observations. p-values were estimated using a moving-block bootstrap (e.g. contiguous 7-day blocks resampled 5000
241 times; (Kunsch, 1989)).

242 **2.2 Site description and climatology**

243 Two populations of *Polylepis pepeii* were sampled at the MNP treeline in October 2012 and July 2019 (3795-4400 m.a.s.l.
244 14°40'-14°43'S; 69°04'-69°06'W; Fig. 1A, C, D). The 2012 campaign took place within an open-canopy south-facing forest
245 (3795-4100 m.a.s.l.), while the 2019 collection was primarily located within a closed-canopy west-facing forest called Waca-
246 cocha (named after a nearby lagoon; 4000-4400 m.a.s.l. Fig. 1D). The forests were largely monospecific, dominated by
247 fragmented patches of *P. pepeii*, and a small number of *Gynoxys compressissima* trees. This treeline is characterized as Alto-
248 Andino Yungueño vegetation (Upper Andean Yungas) with a seasonally humid climate illustrated by the monthly climatology
249 (Fig. 1B)

251 There is a distinct wet season from October-April and dry season from June-August at this site (Fig. 1B). 90% of annual rainfall
252 occurs during the wet season with an average of 1045 mm per month and a mean temperature range between 5-7 °C. In contrast,
253 the dry season is characterized by mean precipitation totals of 95 mm and cooler average temperatures between 2.2-3.1 °C
254 (June-August). October and November are the warmest months of year with maximum temperatures around 14.5 °C (austral
255 spring), but precipitation totals peak in January with an average of ~1900 mm (austral summer). The coldest and driest month
256 of the year is July when minimum temperatures and precipitation are as low as -8.3 °C and 65 mm, respectively (Fig. 1, A1,
257 austral winter). There is a marked seasonality in diurnal temperature range with smaller differences in minimum and maximum
258 temperatures during the peak wet -season (~14.5 °C, December-March; Fig. A1).

Formatted: Border: Top: (No border), Bottom: (No border), Left: (No border), Right: (No border), Between : (No border)

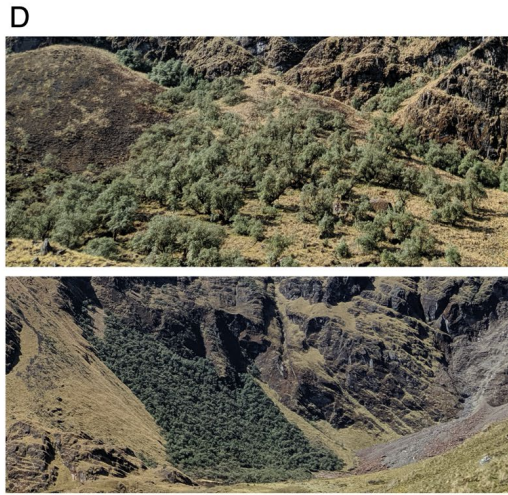
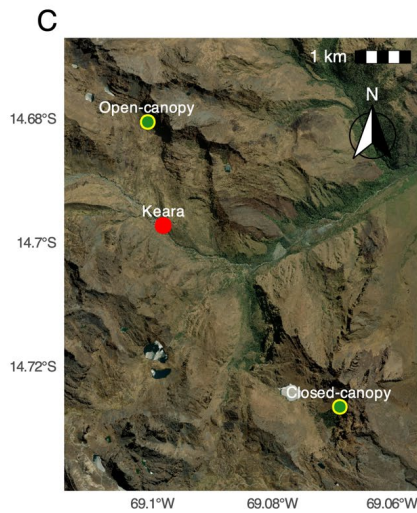
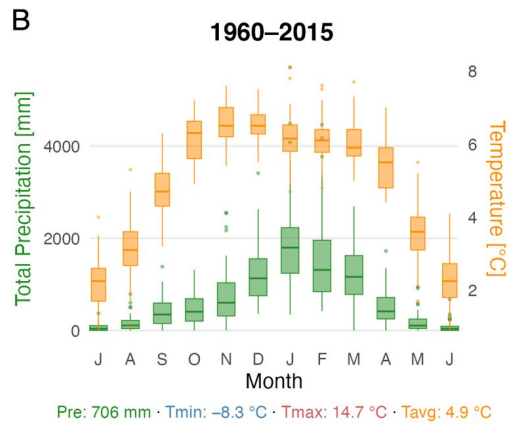
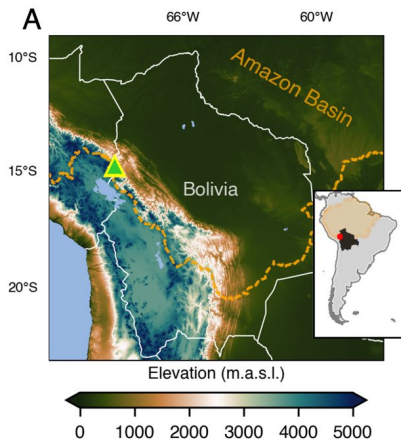
Formatted: Font color: Text 1

Formatted: Font color: Text 1

Formatted: Font color: Text 1

Formatted: Border: Top: (No border), Bottom: (No border), Left: (No border), Right: (No border), Between : (No border)

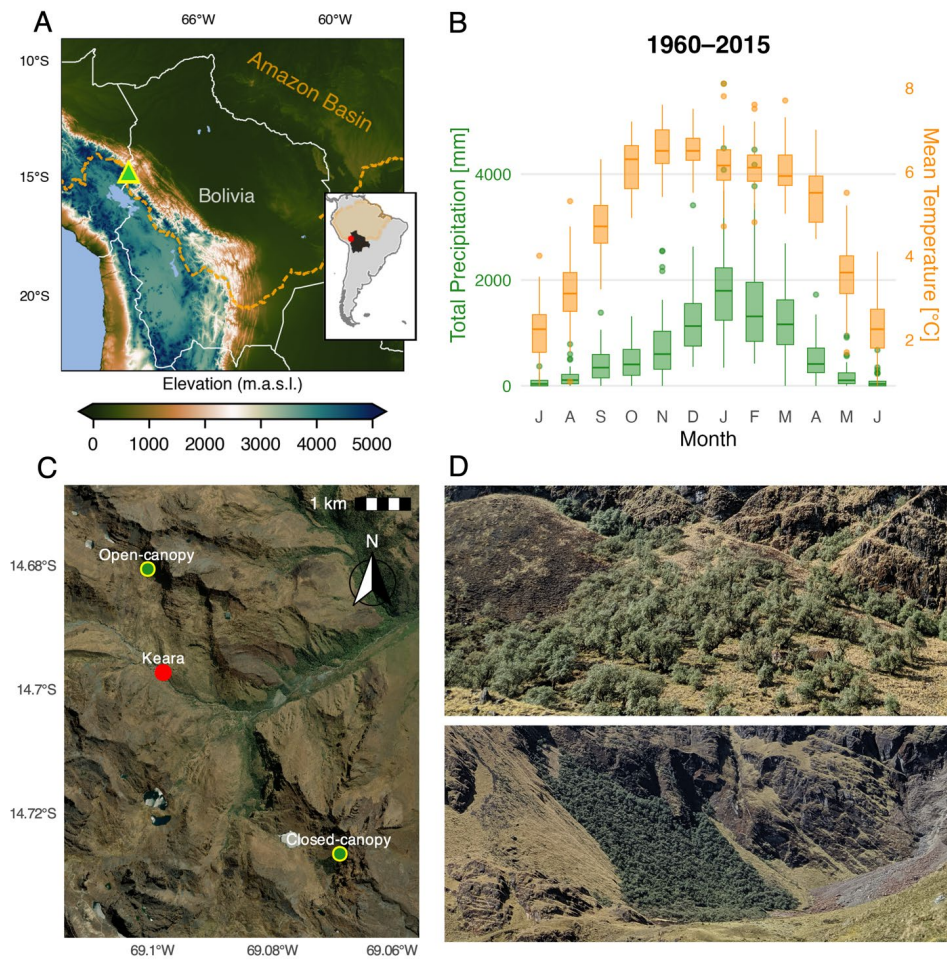
Formatted: Border: Top: (No border), Bottom: (No border), Left: (No border), Right: (No border), Between : (No border)



259

260 Specifically, minimum temperatures range from -2.2 °C to 0 °C and maximum temperatures from 12 °C to 14.5 °C during the
261 wetter months of October-April. Diurnal temperature differences are largest between June-August (~20°C) with minimum
262 temperatures ranging from -7 °C to -8.3 °C and maximum temperatures between 12.5 °C to 13.3 °C.

Formatted: Border: Top: (No border), Bottom: (No border), Left: (No border), Right: (No border), Between : (No border)



263

264 **Figure 1: (A) Location of *Polylepis* site in the Eastern Cordillera of the Andes-Amazon ecotone in Bolivia. The**

265 **orange dotted line (and orange shading in the inset map) represent the spatial limits of the Amazon Basin. The elevation**

266 **map was generated using the “ETOPO-1” model — ([https://www.ncei.noaa.gov/products/etopo-global-relief-](https://www.ncei.noaa.gov/products/etopo-global-relief-model)**

267 **[model](https://www.ncei.noaa.gov/products/etopo-global-relief-model)); (B) The monthly climatology for the region of**

268 **Keara between 1960-2015. Monthly distribution of mean temperature and total precipitation (1960-2015) in Keara was**

269 **generated using the nearest temperature CRU gridpoint (14.75°S, 69.5°W) and total precipitation is reconstructed**

270 **precipitation from the Italaque station (15.48°S, 69.03°W). The average temperature (Tavg), mean precipitation**

271 **(Pre), and range of minimum and maximum temperatures (Tmin, Tmax) for the study period are included. (C) Aerial**

Formatted: Border: Top: (No border), Bottom: (No border), Left: (No border), Right: (No border), Between: (No border)

Formatted: Border: Top: (No border), Bottom: (No border), Left: (No border), Right: (No border), Between: (No border)

272 view of the sampling locations near the community of Keara, and the MNP treeline (D) photos of open-canopy (top)
273 and closed canopy (bottom) forest patches sampled at altitudinal treeline in Bolivia's MNP (~~~3700~~3800-4400 m.a.s.l.).
274 The basemap in (C) was obtained through opensource ESRI images.

275 2.3 Wood processing and anatomical analyses

276 Tree-ring samples from at least 30 living *P. pepei* were collected using a 2-threaded 16-inch increment borer (5 mm in
277 diameter) in October 2012 and July 2019. Two to four cores were extracted from varying directions within the stem (north,
278 south, east, and/or west radii) in an effort sample an accurate representation of radial growth. Trees were cored at breast height
279 (1.2 meters), or near the base of the largest stem for multi-stemmed trees (~30 cm). During the 2019 field campaign, tree-
280 diameter was also measured at the height core samples were sampled (1.2 meters on average). Tree-ring cross sections from 3
281 recently dead trees were sliced using a gas-powered chainsaw or a standard saw-tooth blade.

282
283 Wood samples were shipped from the National Herbarium of Bolivia in La Paz to the Lamont-Doherty Earth Observatory
284 (LDEO) in NY, USA for dendrochronological analysis. Cores and cross sections were finely sanded up to 1000 grit using an
285 orbital sander and manually polished with microfiber paper. Most samples had surficial color differences within the stem,
286 mainly reflecting transitions between the heartwood (functional xylem near the pith, darker color) and sapwood (the active
287 xylem beyond the cambium layer, lighter color).

288
289 *P. pepei* is an angiosperm with diffuse porous wood anatomy, which is typicallyparticularly harder to cross-datethan 'ring
290 porous' wood, due to less distinct boundaries between the latewood of the prior year growth ring and the earlywood of the
291 currentnext year (Fig. A2). To aid in identifying anatomicalpropertiesringboundaries in the wood, -histological (micro) cuts
292 were performed according toa single cross-section following the techniques described in von Arx et al. (2016) using a WSL
293 Core microtome (<https://www.wsl.ch/en/services-produkte/microtomes/>). *P. pepei* tree rings feature large, semicircular vessel
294 elements in the earlywood that taper tangentially in size towards the transition to latewood, which has thicker, fiber-like
295 tracheid cells (Fig. A2-B). High-resolution images of the thin sections were captured using an Echo Revolve R-4 microscope
296 camera, with a magnification of 40X. Further information regarding the wood anatomy of this species is included in the
297 Appendix (Fig. A2).

298 2.4 Tree-ring width chronology development

299 Tree rings from 51 *P. pepei* samples from 28 living and 3 dead trees (31 trees total (51 radii)) were dated visually using standard
300 dendrochronological techniques (Stokes and Smiley, 1968). Each wood sample was scanned using an Epson Expression
301 11000XL scanner at 3200 dpi resolution. RW was measured digitally using the *CooRecorder* image analysis program (Cybis
302 Elektronik, 2010) and statistically crossdated using the program COFECHA (Holmes, 1983) and dplR package in R (Bunn,
303 2008). To independently confirm annual periodicity of the growth rings, radiocarbon dating was conducted on a cross-section
304 sample (SP20X; Fig. A2) collected in 2019 in the closed-canopy forest. Individual growth rings associated with the years 1957,

Formatted: Border: Top: (No border), Bottom: (No border),
Left: (No border), Right: (No border), Between : (No border)

Formatted: Border: Top: (No border), Bottom: (No border),
Left: (No border), Right: (No border), Between : (No border)

1958, 1962, 1963, 1964, 1965, 1971, and 1972 were sliced, extracted for cellulose, and processed for modern radiocarbon analyses. All radiocarbon measurements were compared to the monthly SH $\Delta^{14}\text{C}$ radiocarbon curve (1950-2019 C.E.) from the designated atmospheric Zones 1-2 and 3 (SH Zone 1-2; Hua et al., 2022). Further details on the radiocarbon analyses and earlier iterations of the Keara RW chronology can be found in the Appendix (Fig. A2-CA2C).

Once final calendar dates were assigned to the tree-ring samples, the Schulman convention (Schulman, 1956), which assigns each ring date to the year growth began, was applied. Individual RW time series were detrended conservatively with age-dependent cubic splines using the 'dplR' package in R (initial spline stiffness of 60 yrs) (Bunn et al., 2008; Cook and Peters, 1981; Melvin, 2004). Standardized indices were generated by taking the ratio of the fitted and observed RW values of detrended time series and combined using a robust Tukey bi-weight mean to produce a dimensionless 'standard' RW chronology (Cook et al., 1990). For the residual chronology, autocorrelation was removed from the series using autoregressive modelling determined by the Akaike Information Criterion (Akaike, 1974). A third chronology of average (raw) RW was also generated to review the absolute growth of these trees at treeline. The final RW-chronologies (raw, standard and residual) represent the RW for entire *P. pepei*-RW network (2012 and 2019 tree samples) and thus variance stabilization was applied to account for temporal changes in sample depth (Frank et al., 2006). The standard RW chronology was primarily used for changepoint and RW-climate correlation analyses, (section 2.5), and the residual chronology was used for i.) identification of small or large outliers in the chronology (top 5th and 95th percentiles) and ii.) analyses of the growth response of *P. pepei* to detrended monthly and residual climate and extreme ENSO events (see section 2.6).

The subsample signal strength (SSS) calculation was used to estimate the minimum sample size required to maintain a growth determine how well the available tree-ring samples represent the common growth signal (Wigley et al., 1984) of the *P. pepei* population (i.e. site) (Cook and Pederson, 2011). SSS considers quantifies the strength of the shared variance through time by incorporating the number of cores per tree, the number of individual trees, and the mean interseries correlation among RW series to determine how well the available samples reflect the growth signal of the population (i.e. site). An SSS value threshold of 0.85 (or better) is a common threshold commonly used in dendrochronology and represents signifies the period years when sample size replication is adequate and the common RW signal chronology is considered robust (see discussions Buras et al., (2017) and Wigley et al. (1984) for more details). An annual SSS Index was generated using the 'dplR' package in R (Bunn, 2008).

2.5 Changepoint detection

The period in which SSS was greater than 0.85 was used for changepoint analyses of the raw and standard RW chronologies to detect abrupt shifts in radial growth before and after low-frequency is removed (i.e. detrending). The Pettit's (1979) changepoint detection test was applied to the raw (radial) using the 'trend' package in R (Pohlert, 2016) which identifies a single year when the median tendency of the RW chronology to detect the timing of recent trends in growth is significantly

Formatted: Border: Top: (No border), Bottom: (No border), Left: (No border), Right: (No border), Between : (No border)

Formatted: Border: Top: (No border), Bottom: (No border), Left: (No border), Right: (No border), Between : (No border)

338 higher or lower after the changepoint. Significance of the RW trend after for the post-changepoint ($p < 0.05$) period was
339 determined by evaluated using the non-parametric Mann-Kendall test on the estimated Sen's slope (Sen, 1968). Changepoint
340 analyses was conducted using the 'trend' package in R (Pohlert, 2016).

341 2.5.6 Climate-growth analyses

342 To explore the climate sensitivity of *Polylepis pepeii* at the treeline, we correlated annual RW with local monthly and seasonal
343 precipitation, and minimum, maximum, and mean temperature and precipitation for the period 1960-2015. Monthly (1960-
344 2015; see Section 2.2). Correlations were evaluated using a 24-month window spanning from prior July to current June to
345 account for lagged climate effects on *P. pepeii* RW. Long-term and inter-annual growth response was assessed by correlating
346 i.) standard RW with mean (raw) climate, and ii) residual RW with linearly detrended climate respectively. 3- and 4-month
347 seasonal climate correlations (standard and residual) were calculated to determine whether growth at this site is influenced by
348 cumulative rather than monthly temperature data (T_{avg} , T_{min} , T_{max}) was from the nearest CRU gridpoint to our site: 14.75°S,
349 69.25°W, while monthly and precipitation (Pre) was obtained from local station data (see section 2.2). Monthly conditions.

350
351 Pearson correlations (r) were computed with the estimated using stationary bootstrap method block-bootstrapping methods and
352 implemented with the 'boot' package in R: (Canty and Ripley, 2017). This technique resamples contiguous, randomly-
353 sized blocks of data ($n=1000$) at varying block size times to preserve autocorrelation and quantify the uncertainty of the RW-
354 climate relationship (see Politis & Romano 1994). Significance of the climate-growth relationship was inferred from the two-
355 tailed 95% confidence intervals of the median bootstrapped correlation (i.e., 95% CI excludes zero). Due to the covariance
356 between temperature and precipitation in this region, we used bootstrapped partial correlations (r_p) to evaluate the independent
357 effect of one variable on RW (e.g. temperature), while controlling for the other (e.g. precipitation). Following methods of
358 Meko et al. (2011), partial correlation coefficients for RW-temperature were obtained by: i.) first performing a linear regression
359 between RW and precipitation and ii.) calculating bootstrapped correlations between temperature and the residuals from this
360 regression. The results after removing the influence of precipitation, partial correlations represent the distinct portion of RW
361 variability that is explained by precipitation. Thus, partial correlations show the distinct relationship between RW
362 and monthly temperature while controlling for the influence of precipitation.

363
364 Spatial RW-Climate correlations across tropical south America were used to assess the extent and magnitude of the climate
365 sensitivity of the standard RW chronology to regional temperature (T_{max} and T_{min}) and precipitation signals of the RW
366 within tropical south America. Seasonal climate windows selected variability. The seasonal window for the spatial analyses
367 were each climate variable was inferred from the significant monthly climate-growth relationships. Spatial and the results from
368 3-to-4-month standard and residual correlations with precipitation. Precipitation correlations were conducted using the gridded
369 CHIRPS dataset for the 1981-2015 period (see section 2.2). Otherwise, all monthly and (seasonal) spatial local climate-
370 growth analyses which used reconstructed station data and spatial temperature (gridded CRU data) correlation analyses (RW

Formatted: Border: Top: (No border), Bottom: (No border),
Left: (No border), Right: (No border), Between : (No border)

Formatted: Border: Top: (No border), Bottom: (No border),
Left: (No border), Right: (No border), Between : (No border)

371 ~~vs. climate) were~~was between 1960-2015. Field significance was assessed using a binomial test (e.g. –the probability that *n*
372 number of grid-cell correlations were significant by chance (raw $p < 0.05$) due to the high number of comparisons; see: Livezey
373 & Chen, 1983).

374
375 Linear trends in the ~~local~~(seasonal) climate (1960-2015) were assessed using the Sen’s slope estimator (section 2.4), and
376 significance was evaluated using Mann Kendall tests. Slopes were reported as the average change in climate in units per decade
377 (Fig. A4). Annual and seasonal (October-April; June-August) trends of diurnal temperature anomalies (DTR) were also
378 evaluated for the same period. Additionally, monthly anomalies of ~~T_{min}~~minimum and ~~T_{max}~~maximum temperature were
379 calculated relative to the 1901-2015 CRU baseline (full temporal extent of CRU data) to illustrate long-term temperature
380 variability during the wet and dry season (Fig. A5-BC).

381 2.6.7 Superposed Epoch Analysis

382 ENSO varies between warmer (El Niño) and cooler (La Niña) SST phases (Ropelewski and Halpert, 1987) in the Pacific
383 Ocean, and both extremes substantially impact precipitation and temperature conditions over tropical South America. To
384 investigate the effects of extreme ENSO events on tree-growth, Superposed Epoch Analysis (SEA) was performed on the
385 residual RW timeseries (Fig. 2D) using the method originally described by Haurwitz and Brier (1981) and modified by Rao
386 et al. (2019). SEA is widely used to statistically determine whether the effects of episodic events (e.g. extreme climate events)
387 on a response variable (in this case RW) are statistically significant or due to random noise. The Rao method uses 1000 random-
388 sample double bootstrapping to quantify the RW response at the time of the event (lag= 0) and several years after (in this case
389 four years).

390
391 We analyzed twenty-six years of RW based on the top-ranked December-February (DJF) El Niño and La Niña events ($n=13$
392 each) listed by the National Oceanic and Atmospheric Administration’s Physical Science Laboratory (NOAA-PSL:
393 <https://psl.noaa.gov/ens0/>). These ranked DJF years are determined by NOAA-PSL with the multivariate ENSO indices (MEI;
394 1871~2024). MEI reflects the principal components, or dominant modes, of the entire tropical Pacific ENSO domain (30°N-
395 30°S, 100E°-70°W) rather than any one region (e.g. Niño 3.4) and integrates observations of sea level pressure (SLP), SSTs,
396 meridional (north-south) wind, and outgoing longwave radiation (see Wolter and Timlin, 2011). Extreme years are defined by
397 Pacific SST anomalies during DJF, coincidentally when ENSO is phase-locked with the peak monsoon season (Rasmusson and
398 Carpenter, 1982). ~~Annual Pre (station data; 1960-2015) and CRU precipitation and Tavg (nearest gridpoint 1901-2018) were~~
399 ~~plotted to determine the average climate during years of known ENSO DJF events near Keara.~~ The list of DJF- ENSO-events
400 obtained from NOAA-PSL are included in Appendix Table A1.

Formatted: Border: Top: (No border), Bottom: (No border),
Left: (No border), Right: (No border), Between : (No border)

Formatted: Border: Top: (No border), Bottom: (No border),
Left: (No border), Right: (No border), Between : (No border)

3 Results

3.1 Growth decline in a *P. pepei* tree-ring chronology

The *P. pepei* RW chronology from covers the MNP treeline spans from period 1850-2018 and consists of 51 tree-ring samples (31 individual trees) from open and closed-canopy forests near Keara the MNP treeline (Table 1; Fig. 2). Radiocarbon and standard dendrochronological methods confirmed the growth rings are these trees form annual rings and reflect high-frequency patterns of high and low growth through timeshare a common growth signal in this region (Figs. 2A, C, D). Site metadata and RW chronology statistics for the *P. pepei* network are summarized in Table 1.

Table 1. Summary of *P. pepei* tree-ring sample location, age, sample size, and mean correlation among RW timeseries. The RW chronologies represent the entire collection of cross-dated *P. pepei* samples in Keara obtained in both 2012 and 2019.

Site	Location (elevation)	<i>n</i> trees (<i>n</i> samples)	Mean age [yrs]	Timespan	Mean RW Correlation [\bar{r}]	Mean DBH [cm]
Open-canopy forest (south-facing)	14°40'S 69°06'W (3795-4100 m.a.s.l.)	16 living 2 dead (33)	89	1850-2018	0.53	24 cm (<i>n</i> =6 trees) *
Closed-canopy forest (west-facing)	14°43'S 69°04'W (4000-4400 m.a.s.l.)	12 living 1 dead tree (18)	101	1871-2018	0.44	31 cm
Full network (mean Raw, standard, residual chronologies)	-	31 (51)	93	1850-2018	0.50	30 cm

~~Table 1. Summary of *P. pepei* tree-ring sample location, age, sample size, and mean correlation of RW timeseries per site. *DBH information is only from the samples collected in 2019 which included 6 trees from the open-canopy forest and 13 trees from the closed-canopy site. The final RW chronologies represent the entire collection of *P. pepei* samples in Keara obtained in both 2012 and 2019.~~

~~Due to extreme suppression in radial growth (Fig. 2B), only one or two cores per tree (out of three total) were able to from the living trees could be measured and included in the final RW chronologies. Despite the complex anatomy of *P. pepei*, the cross-dated and used for the final RW datasets. A recent decrease in radial growth was observed in samples from both the open-canopy (18 trees) and closed canopy (13 trees) sites (Fig. samples 2A). The entire Keara *P. pepei* network (mean raw RW:~~

422 Fig. 2A) has been declining steadily since the 1960s, especially after 1996 ($p=0.01$), with a less pronounced trend in the
423 standard RW series (Fig. 2AC).

424
425 Despite difficulties with crossdating due to suppressed tree rings, the entire network shared a coherency in the RW patterns
426 with a mean inter-series correlation of $\bar{r} = 0.50$ for the 1850-2018 period ($n=51$ samples, 31 trees). The SSS metric indicated
427 the common growth signal was particularly robust ($SSS > 0.85$) between 1900-2018 when the sample size was greater than 17
428 (Fig. 2C). The oldest living tree sampled was 168 years of age from the open-canopy forest. The average age of the trees was
429 93 yrs. The years and the average radial growth rate between 1850-2018 was ~ 1.040 mm yr⁻¹. DBH measurements in 2019
430 (6 trees in the open canopy and 13 in the closed canopy site) confirmed these trees were slow-growing with stem diameters
431 ranging from 10 cm to 54 cm (mean DBH 30 cm). The sub-sample signal strength indicated the RW chronology is particularly
432 robust between 1900-2018 when sample size exceeds 17 ($SSS > 0.85$ Fig. 2C).

433
434 *P. pepei* RW at this treeline has been declining steadily since the 1960s (Fig 2.A, C). A changepoint in the raw RW chronology
435 was detected in 1993 ($p=0.0019$), with a significant decline of 0.02 mm yr⁻¹ after 1994. This trend in absolute growth is evident
436 in both the open-canopy and closed-canopy forests at the site (Fig. 2A). Although a non-significant changepoint in the standard
437 RW chronology was detected in 1962 ($p=0.062$), two-tailed Mann-Kendall tests determined the negative slope between 1963-
438 2018 was significant (-0.007 units yr⁻¹, $p < 0.001$; Fig. 2C). Years with extremely large RW (95th percentile) included the
439 1951/52 and 1965/66 growth years (Fig. 2D) which occur before and after a visible growth suppression during the mid-to late
440 1950s (Fig. 2 A, C). Tree rings that began forming in 1906 or 1945 had extremely low values of RW indicating unfavorable
441 growing conditions during the growth year.

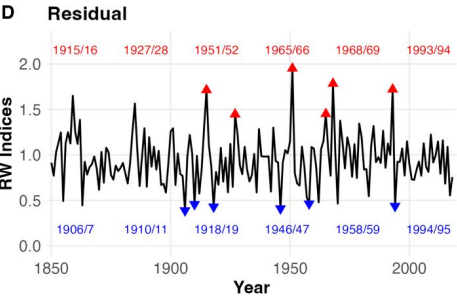
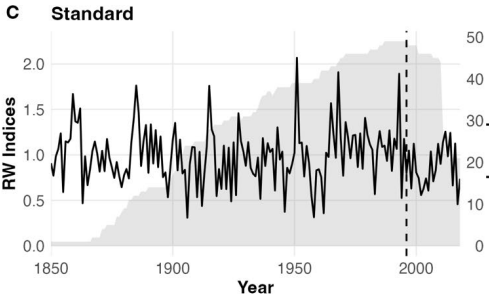
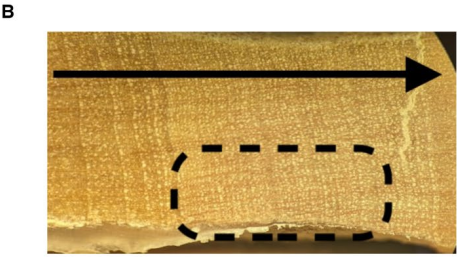
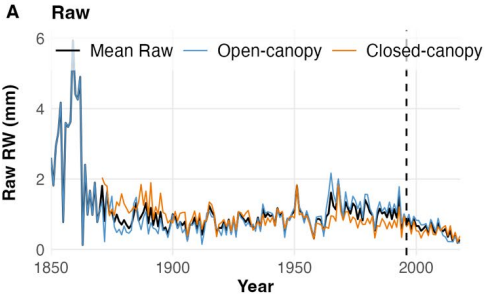
Formatted: Border: Top: (No border), Bottom: (No border),
Left: (No border), Right: (No border), Between : (No border)

Formatted: Font color: Text 1

Formatted: Font color: Text 1

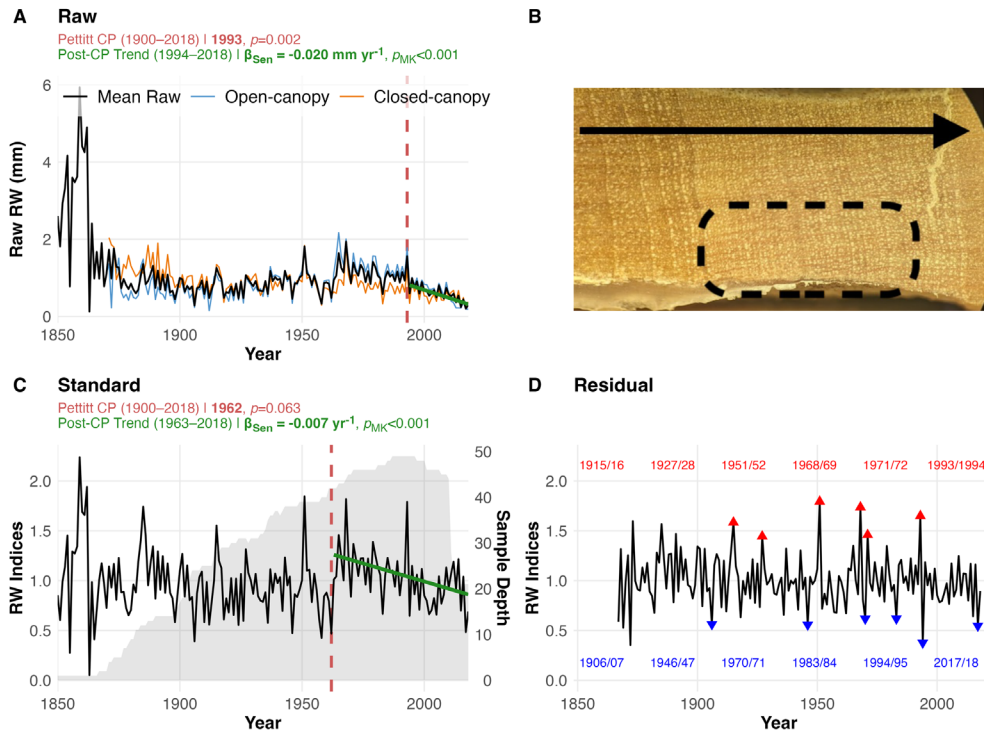
Formatted: Border: Top: (No border), Bottom: (No border),
Left: (No border), Right: (No border), Between : (No border)

Formatted: Border: Top: (No border), Bottom: (No border), Left: (No border), Right: (No border), Between : (No border)



443
444
445
446
447

Formatted: Border: Top: (No border), Bottom: (No border), Left: (No border), Right: (No border), Between : (No border)



448
 449 **Figure 2.** The (A) Raw (C) Standard and (D) Residual RW chronologies of *P. pepei* in Keara. The chronologies (1850–
 450 2018) are plotted using the Schulman convention (*i.e.*, anchored on the year of initial ring formation; see section 2.3).
 451 (A) There has been a distinct decline in raw (radial) RW since the 1996/1997 growth-year (change point is indicated by
 452 the black-dotted line. (A) This decline ($p=0.01$) was evident in both the open-canopy (blue line) and closed-canopy
 453 (orange line) forests that were sampled. (B) An image depicts a core sample where several rings are suppressed within a
 454 4 mm distance (dashed circle). The black arrow indicates the direction of radial growth for this core (from left to
 455 right). (C) The standard RW is plotted with the mean sample-depth of the full network through time (grey-shading).
 456 Triangles Blue and red triangles on the residual timeseries (D) signify the years within the top 5th (six smallest growth
 457 rings; Blue color) and 95th (*i.e.* largest growth rings; red color) percentiles of RW since 1900 ($SSS > 0.85$). Since the tree
 458 rings are estimated to form during the wet season (two-calendar years ~October–April), both years are labeled in the
 459 colored text (and ordered chronologically), within the plot (D). Vertical red lines signify the significant change points
 460 detected in the raw and standardized RW chronologies (1900–2018; $SSS > 0.85$), while the green solid lines represent
 461 the trends after the change point estimate via Sen’s slope. Change point and trends statistics for the raw and standard
 462 RW chronologies are included in the subtitles for A and C. There was a significant decline in raw (radial) RW after the
 463 1993/94 growth-year (*i.e.* 1994–2018) and between 1963–2018 in the standard RW chronology.

Formatted: Border: Top: (No border), Bottom: (No border),
 Left: (No border), Right: (No border), Between: (No border)

Formatted: Border: Top: (No border), Bottom: (No border),
 Left: (No border), Right: (No border), Between: (No border)

3.2 Monthly and seasonal climate-growth relationships at Keara's treeline

The climate sensitivity of *P. pepei* RW to local climate between 1960-2015 is illustrated by bootstrapped correlations between with monthly Pre, Tavg, Tmin, mean precipitation and Tmax in temperature timeseries (1960-2015; Fig. 3-, A3). *P. pepei* RW (standard chronology) positively correlates with Pre benefits from higher rainfall in the months of December-April (Pre lag=1, $r=0.39$ for February; Fig.3A). This forest had a more significant RW response to cumulative rather than monthly precipitation variability during the wet season (Fig.3A). There are significant, with the highest correlations between RW and prior (lag=1) observed for the 4-month December-March precipitation ($r=0.37$ for January). Correlations with prior-year December (season (DJFM lag=1, $r=0.20$)) weakened when controlling for Tavg, but current year November Pre remains robust ($r=0.42$, $p=0.27$). Fig. 008; Figs. A3A, A4A shows December-March (-B). DJFM) precipitation significantly decreased over the 1960-2015 period at this site at a rate of ~6 mm per decade at the same time there was an observed decline in *P. pepei* RW (Fig. 2A). decade⁻¹ after 1960 (Fig. 4A), but residual RW-precipitation correlations remained significant after climate trends were removed (Fig. A4B).

RW is

In general, wet season precipitation is significantly and negatively correlated to prior-year Tavg DJFM (with temperature at this treeline (Oct-April $r=-0.21$ in March to $r=-0.34$ in February, $p<0.05$), -31 , $p=0.02$). However, after controlling for precipitation effects, partial correlations for Tavg revealed a on RW variability, partial correlations revealed a robust and independent relationship between RW and current-year monthly temperature (i.e. the monthly correlations persist after the covariance with precipitation is removed; Lag=0 Fig. 3B-D). *P. pepei* RW correlates positively with current-year mean and maximum temperatures particularly for the months of April (Tavg $r=0.37$, Tmax=0.38; Fig. 3B, D). The strongest positive, robust relationship ($p<0.05$) with RW current-year correlations with temperature were for the 4-month February to April (FMA) months ($r_p=0.25$ in February to 0.37 in April). *P. pepei* RW also correlates positively with FMA Tmax (Fig. 2D); May season, emphasizing the importance of late- summer temperature variability for tree-growth at this site (FMAM Tmax, lag=0, $r=0.47$, Fig. A5H). There was weak evidence of a decreasing trend FMAM maximum temperatures for the analyses period $-0.06^{\circ}\text{C decade}^{-1}$, $p=0.17$; Fig. 4D).

Monthly residual correlations showed *Polylepis pepei* RW was primarily sensitive to interannual temperature variability at this site (Figs. 3B-C, A3B-C, Tavg, Tmax, Tmin). However, prior-year correlations with monthly Tmax and Tavg decreased after accounting for lagged precipitation effects on RW (Fig. 3B and D lagged partial correlations). Lagged minimum temperature variability, however, had a distinct and significant impact on RW (Tmin lag=1, Figs. 3C, A3C). Negative correlations were found between RW and prior-year wet season temperature variability near our site on current year RW as well season minimum temperatures (NDJF lag=1; $r=-0.40$; Fig. A4F). Although there were no significant trends in FMA Tavg between 1960-2015 (Fig. A4 B), there was a significant decrease of Tmax FMA of nearly 0.1°C per decade (Fig. A4 D, $p=0.05$ FMAM mean and max temperature for the 1960-2015 period ($p > 0.16$; Fig. 4B, C), NDJF minimum temperatures significantly

Formatted: Border: Top: (No border), Bottom: (No border), Left: (No border), Right: (No border), Between : (No border)

Formatted: Border: Top: (No border), Bottom: (No border), Left: (No border), Right: (No border), Between : (No border)

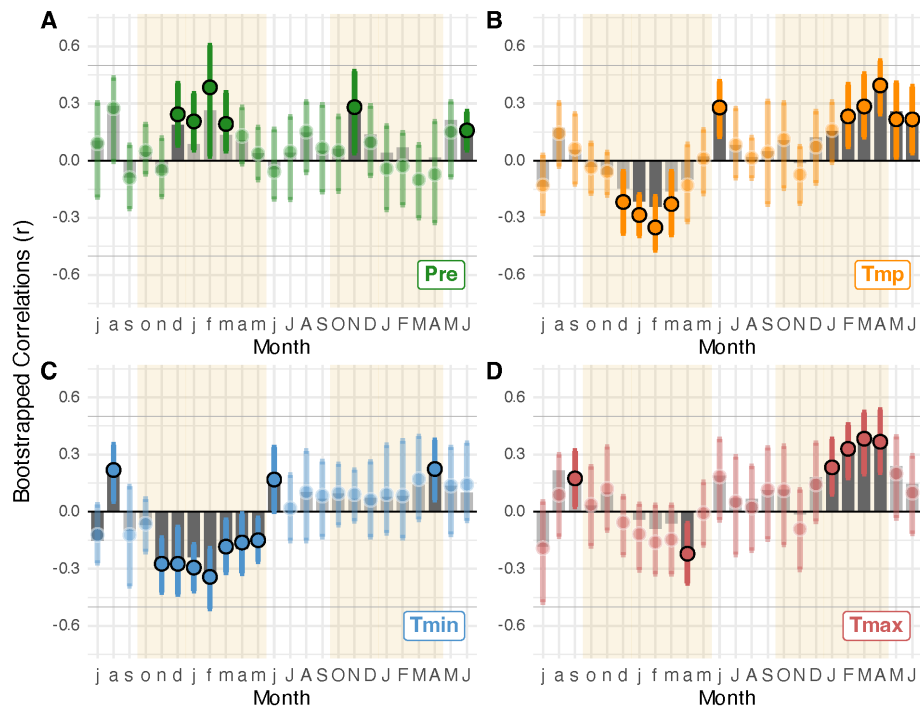
498 increased at a rate of $0.15^{\circ}\text{C decade}^{-1}$ ($p=0.02$, Fig. 4C). In summary, *Polylepis pepeii* RW was limited by minimum and
499 maximum temperatures for distinct seasons (e.g. positive relationship with FMAM Tmax lag=0 vs. negative relationship with
500 NDJF Tmin lag=1).

501
502 Unlike Tavg, partial correlations indicate RW correlations with prior-year Tmin (Fig. 3C) are significant independent of
503 precipitation variability (i.e. the negative signal persists even when the covariance with precipitation is removed). Negative,
504 significant correlations were found between *P. pepeii* RW and prior November–March Tmin (NDJF; $r=-0.28$ in November to
505 $r=-0.35$ in February). It is interesting to note an extreme cold period near Keara during the late 1950s (Tmin, Fig. A5 BC)
506 corresponds with a growth suppression observed in *P. pepeii* RW in Fig. 2A and C. Unlike the decrease observed in Tmax near
507 Keara (FMA), NDJF Tmin significantly increased at a rate of $0.1^{\circ}\text{C per decade}$ ($p=0.02$). In summary *Polylepis pepeii* RW is
508 limited by FMA Tmax (positive, current year relationship) and NDJF Tmin (negative, lagged relationship) for distinct seasons.
509

510 Overall *Polylepis pepeii* RW is larger under wetter and cooler conditions. However, ~~elimat~~ this site experienced significant
511 warming and drying trends since between 1960 (Fig. A4) indicate this 2015 at the same time a growth decline in the treeline
512 is facing a warmer and drier November–March (Pre, Tmin) and a cooler wet to dry ‘shoulder season’ months between
513 February–April (Tmax). As mentioned in Section 2.1, Tavg and Pre are negatively correlated during the wet season (–October–
514 April, $r=-0.27$) in Keara and thus the robust negative correlations between RW temperature (Tmin, Tmax) *P. pepeii* was
515 observed (Figs. 2C, 4A, 4C). Residual climate-growth correlations were significant for the same seasons as the standard
516 correlations, despite the linear trends identified in both mean climate and RW (Fig. 2, 4). These results emphasize the indirect
517 effect of temperature that both long-term and inter-annual climate variability had significant impacts on water availability and
518 thus *P. pepeii* tree-growth RW at this treeline. Seasonal averages of DJFM precipitation, NDJF Tmin and FMA Tmax were
519 selected for spatial correlation analyses for the greater tropical south American region, in the MNP. Further, RW was primarily
520 limited by prior-year wet-season conditions (e.g. ~Nov–March Pre and Tmin lag=1) but was also significantly and positively
521 related to current-year temperature variability (FMAM lag=0).
522

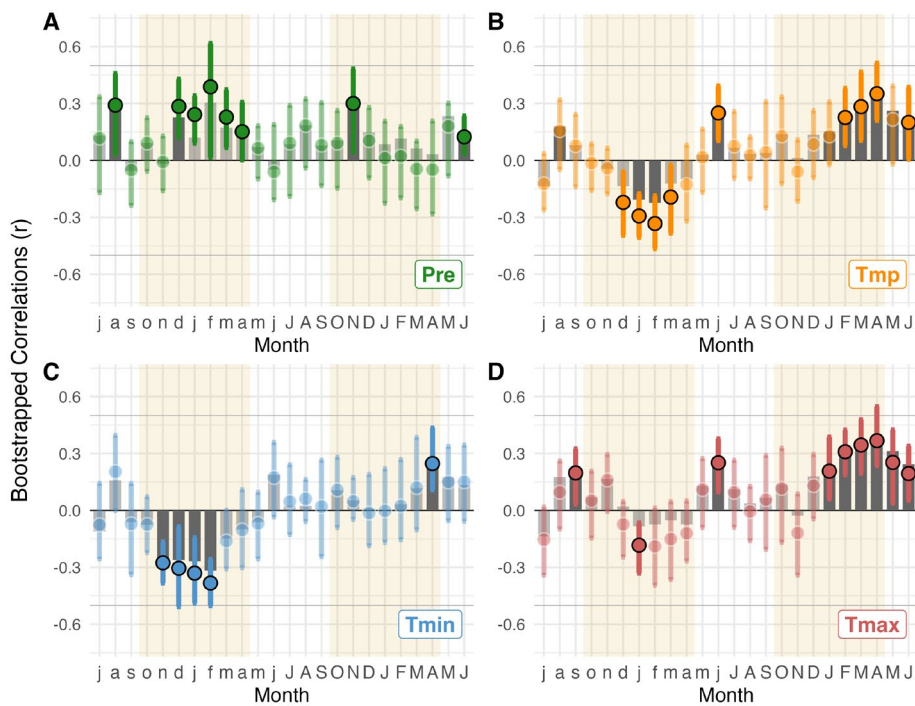
Formatted: Border: Top: (No border), Bottom: (No border),
Left: (No border), Right: (No border), Between : (No border)

Formatted: Border: Top: (No border), Bottom: (No border),
Left: (No border), Right: (No border), Between : (No border)



Formatted: Border: Top: (No border), Bottom: (No border), Left: (No border), Right: (No border), Between : (No border)

Formatted: Border: Top: (No border), Bottom: (No border), Left: (No border), Right: (No border), Between : (No border)

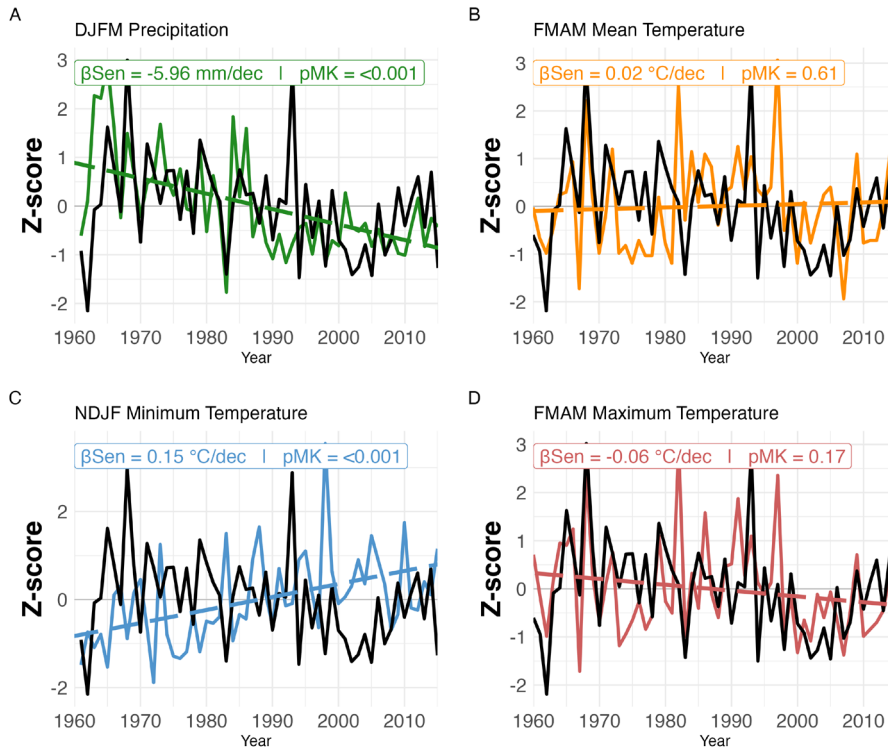


524
 525 **Figure 3: Bootstrapped Standard bootstrapped** correlations between *P. pepei* RW and **average** monthly climate from
 526 1960-2015. The x-axis represents months beginning in Monthly temperature data was from the nearest CRU gridpoint
 527 for our site: 14.75°S, 69.25°W, while monthly precipitation was obtained from local station data. The x-axis covers the
 528 24-month period between July of the prior-year (lag=1, lowercase letters) and extending to June of the current year
 529 (lag=0, uppercase letters). Tan shading indicates the extended wet period (~October–April) wet-season for this region
 530 of the MNP (~October–April). (A:–) Monthly RW-precipitation correlations (green color, precipitation from local
 531 station data., Pre). (B-D:) RW correlations with CRU monthly mean (orange, Tavg), minimum (blue, Tmin), and
 532 maximum temperature grid-points Tavg (orange), Tmin (Blue), Tmax (red). The median Pearson correlation (r) is r
 533 Tmax). Significant correlations are represented by solid-colored circles plotted with upper and lower limits of
 534 confidence intervals. Partial correlations (r_p) are represented by (median Pearson r) or solid grey bars. Solid circles
 535 and bars indicate significant (partial correlations which are, r_p) and inferred from 95% confidence intervals from the
 536 random bootstrapping.

Formatted: Border: Top: (No border), Bottom: (No border),
 Left: (No border), Right: (No border), Between : (No border)

Formatted: Border: Top: (No border), Bottom: (No border),
 Left: (No border), Right: (No border), Between : (No border)

Seasonal climate trends near Keara



538
539 **Figure 4. Z-scored *P. pepei* RW (black lines) and seasonal climate variables (colored solid lines) between 1960-2015.**
540 **The selected seasons were based on the highest and most significant correlations between local climate and RW for this**
541 **period (standard and residual, $p < 0.05$). Lagged DJFM Precipitation is in green (A, lag=1), FMAM mean temperature**
542 **is orange (B, lag=0), lagged NDJF minimum temperature is blue (C, lag=1) and FMAM maximum temperature is in**
543 **red (D, lag=0). Averaged seasonal trends are reported in units of climate per decade (β , colored dashed lines). Mann-**
544 **Kendall tests were used to estimate the two-tailed significance of the linear trend (pMK). Precipitation data is**
545 **reconstructed from nearby station records and temperature data is sourced from the nearest CRU TS 4.08 grid point.**

Formatted: Border: Top: (No border), Bottom: (No border), Left: (No border), Right: (No border), Between: (No border)

Formatted: Font color: Text 1

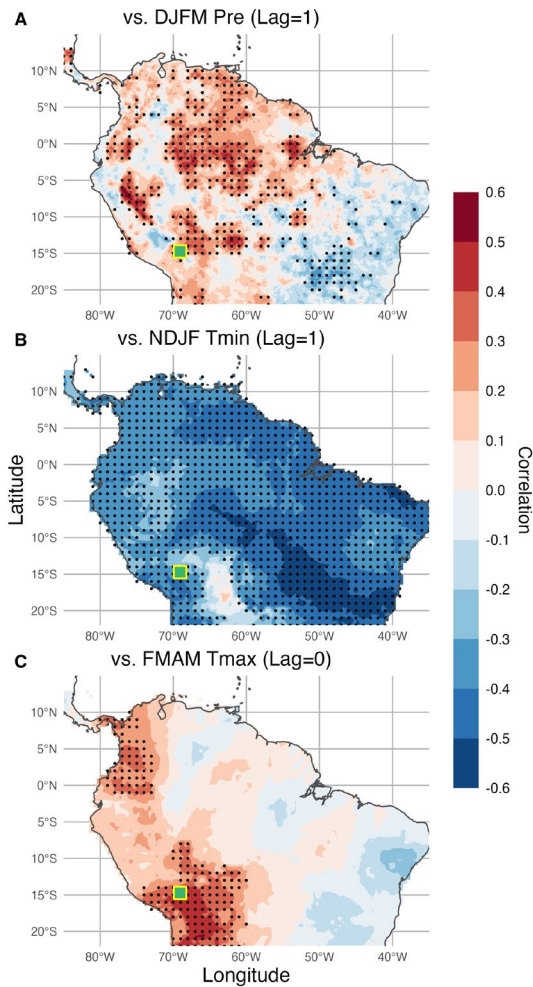
Formatted: Border: Top: (No border), Bottom: (No border), Left: (No border), Right: (No border), Between: (No border)

548 **3.3. *Polylepis pepeii* RW and climate variability across tropical South American climate variability America**

549 Spatial correlations reveal the broader, Figure 5 highlights the regional extent of the seasonal climate signal recorded in the *P.*
550 *pepeii* RW at the **KearaMNP** treeline. (Fig. 4). Binomial field tests indicated the spatial extent of significant correlations (black
551 dots; $p < 0.05$) exceeded what would be expected Gridded DJFM precipitation (lag=1), NDJF minimum temperature (lag=1),
552 and FMAM maximum temperature fields for tropical South America were used for spatial correlation analyses and were
553 limited by chance ($p < 0.001$ for all variables). *P.* the temporal extent of available data (Fig. 5A 1981-2015, Fig. 5B-C 1960-
554 2015). The RW-precipitation correlations reflect the heterogeneity of precipitation variability along the Andes, whereas the
555 temperature fields are more uniform (Fig. 5A vs. Fig. 5B, C). *P. pepeii* RW is positively correlated to prior-year DJFM
556 precipitation (CHIRPS; 1981-2015) rainfall in most of tropical South America for the 1981-2015 period (Fig. 4A5A). The
557 strongest precipitation signal is observed along the eastern flanks of the Peruvian Andes and the northern Amazon Basin in
558 Brazil. ($r = 0.45$ to 0.50). There were significant correlations with wet-season minimum temperature variability for most of
559 tropical South America, especially near southeastern portions of Brazil (NDJF T_{min} lag=1, 1960-2015; Fig. 5B). RW is also
560 positively correlated to FMA T_{max} late austral summer maximum temperature variability in the northern and southern portions
561 of the tropical Andes-Amazon with the strongest values ($r > 0.50$) (FMAM T_{max} lag=0, 1960-2015, Fig. 5C). The highest
562 correlations between RW and maximum temperature were centralized both locally to the site and near the Bolivian Altiplano-
563 ($r > 0.50$). In summary, the relationship between *P. pepeii* RW and large-scale seasonal climate variability was significant for
564 the same seasons identified in the local climate-growth analyses (1960-2015, Figs. 3, A4, A5).

Formatted: Border: Top: (No border), Bottom: (No border),
Left: (No border), Right: (No border), Between : (No border)

Formatted: Border: Top: (No border), Bottom: (No border),
Left: (No border), Right: (No border), Between : (No border)

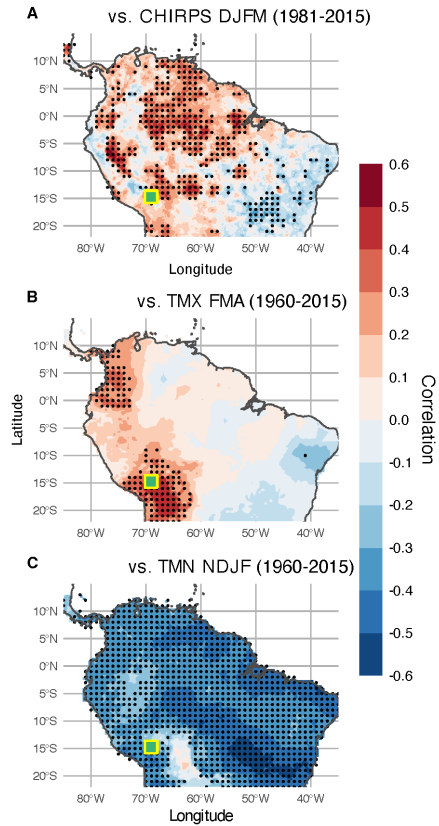


566

567 **Figure 5.** Spatial correlations between *P. pepel* RW and prior year NDJF Tmin (CRU 1960–2015) showed significant and
 568 negative correlations across most of tropical South America (Fig. 4C), especially near southeastern portions of Brazil. The RW-
 569 precipitation correlations also reflect the heterogeneity of precipitation data in mountain areas, whereas the temperature fields
 570 are more uniform.

Formatted: Border: Top: (No border), Bottom: (No border),
 Left: (No border), Right: (No border), Between : (No border)

Formatted: Border: Top: (No border), Bottom: (No border),
 Left: (No border), Right: (No border), Between : (No border)



572

573 **Figure 4. Spatial correlations between *P. pepeii* RW and (A) CHIRPS DJFM precipitation (1981-2015, lag=1), (B) CRU**
 574 **NDJF T_{min} (1960-2015, minimum temperatures (lag=1), and (C) CRU FMA T_{max} (1960-2015, FMAM maximum**
 575 **temperatures (lag=0)) in tropical South America. Black dots represent the areas where there are significant**
 576 **correlations ($p < 0.05$). Binomial field tests indicated the significant grid points ($p < 0.05$). Gridded precipitation analysis**
 577 **was limited to 1981-2015 due to the availability of CHIRPS data (A) while RW-temperature correlations covered the**
 578 **1960-2015 period (B-C, CRU data). There were more significant cells than expected by chance ($p = 0.05$) for all variables**
 579 **(spatiotemporal relationships (binomial field test $\alpha = 0.05$, $p < 0.001$)).**

579

Formatted: Border: Top: (No border), Bottom: (No border), Left: (No border), Right: (No border), Between: (No border)

Formatted: Font color: Text 1

Formatted: Font color: Text 1

Formatted: Font color: Text 1

Formatted: Font color: Text 1

Formatted: Border: Top: (No border), Bottom: (No border), Left: (No border), Right: (No border), Between: (No border)

3.4. Long-term changes in diurnal climate conditions at the Keara treeline

In agreement with the decreased DTR trend observed since 1960, in situ daily temperature loggers independently confirmed that minimum temperatures for the October-April season have increased at this site (Fig. A6 A-C). Minimum temperatures for the October-April season in 2011-2014 ranged from 1.9-2.3 °C and increased to 3°C in 2021-22, which is higher than the 0°C average between 1960-2015 (Section 2.2, Tmin Fig. A1). The distribution of daily wet season minimum temperatures in 2021-2022 was significantly higher than the 2011-2014 seasons overall (bootstrap KS test $p < 0.001$); Fig A6).

3.4

Interestingly, average October-April maximum temperatures recorded by the data loggers ranged 7.2°C-8.2°, which is substantially lower than the 1960-2015 average (Section 2.2, Tmax~13°C; Fig. A1). Daily maximum temperature for the 2021-2022 season was significantly lower than the 2012-13 and 2013-14 seasons ($p < 0.01$), while no significant difference was detected relative to the 2011-2012 season ($p = 0.37$).

The daily data loggers also recorded a significant reduction in relative humidity within the 2011-2022 period (October-April; Fig A6D-F). Relative humidity declined from an average of 98% in 2011-2014 to 90% in 2021-2022, while minimum daily humidity decreased from ~94% to 80% (Fig. A6D, F). Although 2011-12 corresponded to a DJF-La Niña year (Table A1), the distribution of daily relative humidity values during that season was comparable to the 2012-13 and 2013-14 years ($p > 0.05$), and all 3 seasons were more humid than the 2021-22 year (Fig. A6. $p < 0.001$). In fact, almost one third of daily relative humidity values for 2021-2022 (63 days) were below 90% for October-April, while less than 25 days were recorded for the same threshold in the 2011-2014 seasons.

In summary, the long-term warming and drying trends observed in precipitation and temperature between 1960-2015 (Figs. 4, A5) are consistent with in situ measurements of higher temperature and lower relative humidity for 4 distinct October-April seasons between 2011-2022 (Fig. A6).

3.5 Growth response of treeline *P. pepei* to extreme climate events

The impact of extreme DJF-ENSO events on climate and the residual RW chronology is shown in Figure 5. Table A1 lists the years of known moisture/hydroclimate anomalies in tropical South America connected to El Niño (warmer SST) or La Niña (cooler SST) conditions in the Pacific Ocean. Regardless of the time span and spatial temporal resolution, climate datasets show agree that the El Niño-DJF events were linked to drier and warmer conditions at this site, while extreme La Niña-DJF years were wetter and cooler (Fig. 6A, B). SEA of the residual RW response depicts temporal growth anomalies for top 26 ENSO DJF events: 13 El Niño and 13 La Niña (Figs. 6CD). There was a one-year delayed and negative RW response to El

Formatted: Border: Top: (No border), Bottom: (No border), Left: (No border), Right: (No border), Between : (No border)

Formatted: Border: Top: (No border), Bottom: (No border), Left: (No border), Right: (No border), Between : (No border)

611 Niño events, i.e., one year after an event, *P. pepei* showed a significant decrease in radial growth ($\alpha = 0.1$). There was
 612 a significant negative response two and three years after an extreme DJF-La Niña.
 613 SEA results for El Niño DJF years show there was a one-year delayed and negative
 614 Some RW response, i.e., outliers identified in the residual one year after an event, *P. pepei* showed a decrease in radial growth
 615 ($\alpha = 0.1$). Although there was a non-significant growth increase in RW after a La Niña DJF, there was a significant negative
 616 response three years after an extreme DJF-La Niña chronology coincide with years of known ENSO events. (Fig. 5B). It's
 617 interesting to note however, the 2D) The largest growth tree-ring observed in *P. pepei* formed during occurred at the 1950-
 618 1951 wet season and correspond to same time than an extreme DJF-La Niña events event in DJF-1950 and 1951 (Fig. 51 while
 619 the 2C). The smallest (5th percentile) growth ring in 1906-07 occurred the chronology was formed after a major DJF-El Niño
 620 event in 1905. In summary, *P.* (Table 1; Fig 2D). Overall, the inter-annual *P. pepei* RW at the Andes-Amazon treeline has a
 621 lagged significant response to extreme DJF-ENSO conditions.
 622

Formatted: Border: Top: (No border), Bottom: (No border), Left: (No border), Right: (No border), Between : (No border)

Formatted: Font color: Text 1

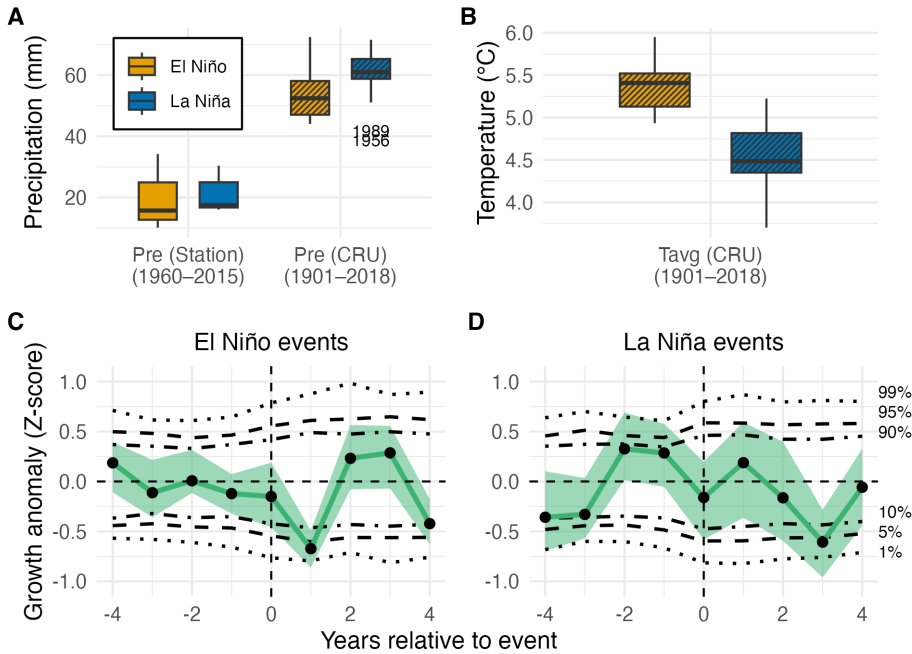
Formatted: Font color: Text 1

Formatted: Font color: Text 1

Formatted: Font color: Text 1

Formatted: Font color: Text 1

Formatted: Font color: Text 1



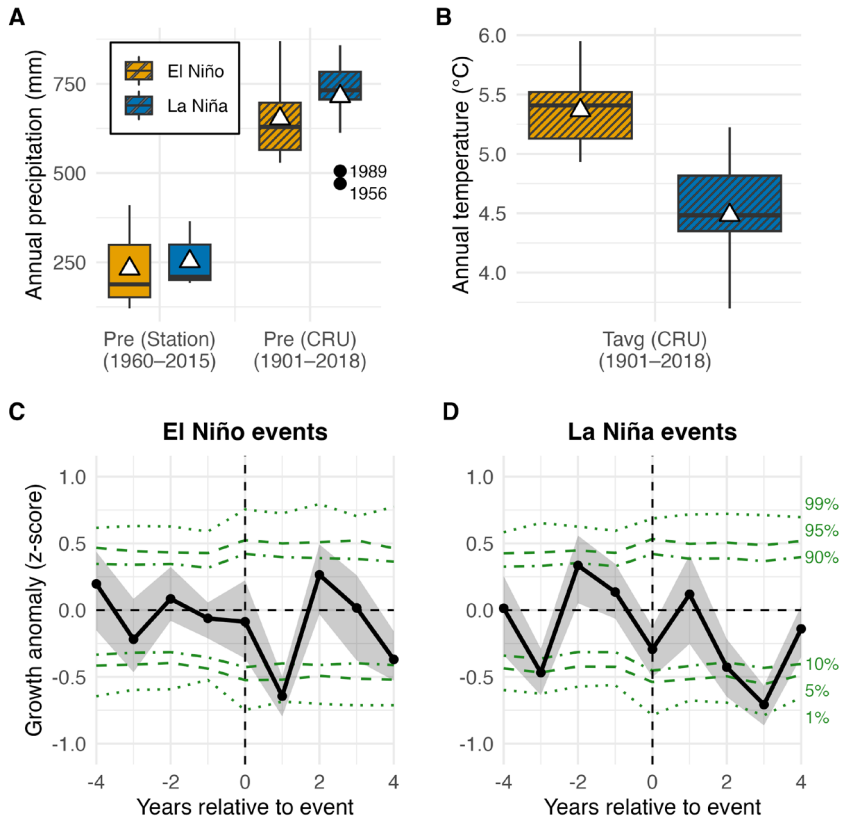
Formatted: Border: Top: (No border), Bottom: (No border), Left: (No border), Right: (No border), Between : (No border)

623

624 To visualize the significant increase of minimum temperatures near Keara in a long-term context, annual and seasonal diurnal
 625 temperature range anomalies were calculated for the full CRU TS 4.08 calibration period 1901-2015 (Fig A5; DTR, Tmin,
 626 Tmax). There was a significant decrease in DTR and an increase in minimum temperature anomalies since the mid-20th century
 627 at this site. The largest decline in DTR was observed for the October-April season at a rate of $-0.197^{\circ}\text{C decade}^{-1}$, though annual
 628 and July-August DTR declined at a similar rate (-0.191°C and $-0.194^{\circ}\text{C decade}^{-1}$ respectively, 1960-2015; Fig. A5).

Formatted: Border: Top: (No border), Bottom: (No border), Left: (No border), Right: (No border), Between : (No border)

629
630



631
632

Formatted: Border: Top: (No border), Bottom: (No border), Left: (No border), Right: (No border), Between : (No border)

633 **Figure 56:** Boxplots showing of annual (A) precipitation and (B) temperature for the 26 years of extreme DJF-ENSO
634 events, using both station and CRU data. Outlier years in the CRU precipitation data are labeled in (A), represented as
635 black dots (A: 1956, 1989). Annual mean climate during El Niño-DJF is represented as orange colors, while La Niña is
636 shown in blue ($n = 13$ years per event). Superposed epoch analysis of the residual RW response between 4 years before
637 and 4 years after the DJF-ENSO events (C, D; black line). The uncertainty of the growth response is depicted as
638 greengrey shading. Horizontal black-green lines represent confidence intervals (the two-tailed significance thresholds: (10-
639 90%, 5-95% 1-99%) based on derived from stationary bootstrapping.

647 4 Discussion

648 4.1. Climate sensitivity and Radial growth decline and climate sensitivity of a tropical treeline site in Bolivia

649 Annual RW chronologies of Here we have generated the first *P. pepei* tree-ring chronology from a high Andean Amazon
650 forest the MNP treeline in Bolivia have been presented and analyzed. This is the first tree-ring longest annual growth record for
651 this species in South America spanning from 1850 to 2018 CE (3795-4400 m a.s.l; 14.75°S). These results provide new
652 information of tree growth and climate dynamics in an understudied biodiversity hotspot in the southwestern Andes-Amazon
653 corridor. We found that *P. pepei* RW is limited by prior-year minimum temperature (negatively) and precipitation (positively)
654 variability during the wet season, leading to larger RW in the subsequent growth year when it was colder and wetter (Figs. 3
655 and 4). There was also a positive relationship between current-year maximum temperature and RW variability between 1960-
656 2015 at this treeline. The lagged RW-precipitation signal is consistent with one of the two *P. pepei* tree-ring studies (lag=1;
657 1969-2004; 16°12S, 68°79W; 4130 m.a.s.l; Jomelli et al. 2012) and several *Polylepis tarapacana* investigations that reported
658 prior-year water availability as a useful predictor of RW (Argollo et al. 2004, Morales et al. 2004, Christie et al. 2009, Soliz et
659 al. 2009, Crispin-DelaCruz et al. 2022, Rodriguez-Caton et al. 2021). The second study of *P. pepei* found that RW was
660 positively correlated to current-year temperature variability (lag=0; 1941-1983; 17°S, 65°39W; 4100 m.a.s.l Roig et al. 2001).
661 However, the dominant and negative relationship between RW and lagged minimum temperature variability has yet to be
662 explored for treeline *P. pepei*.

663
664 The pronounced decline of radial growth in *P. pepei* since 1960 coincided with warmer and drier austral summers at this
665 treeline (~November-March, 1960-2015; Figs. 2C & 4AC). There was also a significant step change and subsequent decline
666 in raw RW after the 1993 growth-ring (Fig. 2A). It is possible that this area was affected by an 8.2 magnitude earthquake ~150

Formatted: Border: Top: (No border), Bottom: (No border),
Left: (No border), Right: (No border), Between : (No border)

Formatted: Font color: Text 1

Formatted: Border: Top: (No border), Bottom: (No border),
Left: (No border), Right: (No border), Between : (No border)

667 km east of the site was recorded in June 1994 (Myers et al. 1995). Although this region of Bolivia is sparsely populated,
668 landslides were reported in southern Peru and Chile, and thus it is possible that slope failures in 1994 occurred near this treeline
669 in Keara Bolivia (Blodgett et al. 1998). This decline also occurred 1 year before the broader study region of Madidi was
670 designated a National Park and the longest record of *P. pepei* RW chronology in South America (1850-2018). This record
671 provides new information about tree growth and climate in September 1995 due to its extremely high levels of biodiversity
672 and endemism for the Southern Amazon. The results herein verify the sensitivity of *P. pepei* tree-ring width at this site to both
673 local climate and environmental disturbances. An altitudinal advance of this treeline is unlikely due to local geomorphologic
674 constraints (Fig. 1D; Macias-Fauria and Johnson, 2013). Further, species-specific thermal niches that are required for seedling
675 establishment and recruitment may be at risk due to the observed increasing temperature trends in recent decades (Kessler et
676 al., 2014; Körner and Hoch, 2023), in an understudied tropical treeline in South America (~3800-4400 m.a.s.l.). The potential
677 human influence on RW for trees. Although the spatial extent of this forest under increased warming and environmental change
678 is uncertain, this study has helped clarify the nature of past and current growth variability of *P. pepei* in this region.

680 Human activity in Andes-Amazon forests should be considered when evaluating the growth patterns at tropical treelines in
681 this region. For the *P. pepei* near Keara, Forest fragmentation was observed in the lower elevation open-canopy forest (3795-
682 4100 m.a.s.l.) and tree-ring samples showed possible evidence of fire scars in the 1940s and clear forest fragmentation related
683 to cattle ranching. This subpopulation is likely more threatened by human activities—small-scale cattle ranching in Keara than
684 the closed canopy site between forest located at higher elevations (4000-4400 m.a.s.l. sampled in 2019 (Fig. 1CD); Fig. 1C,
685 D). Herein, efforts were made to minimize potential impacts of land use and disturbance in field sampling, but ecosystem
686 disturbances in certain regions of the MNP were nevertheless observed (mostly in areas below 2000 m.a.s.l.). Despite the
687 potential for local environmental effects on growth these observations, correlations between *P. pepei* RW and local climate
688 are regional temperature and precipitation variability were robust and may signify a response to regional shifts in larger-scale
689 hydroclimate patterns observed seen in tropical South America (Fig. 5).

691 We found that *P. pepei* RW is limited by prior-year temperature and precipitation variability during the wet season, with larger
692 RW in the subsequent growth year when it was wetter and colder (Figs. 3 and 4). This is consistent with previous studies
693 showing *Polylepis* ring width positively correlated with previous growing season water availability in the Andes (Argollo et
694 al. The MNP treeline, 2004, Morales et al. 2004, Christie et al. 2009, Soliz et al. 2009, Crispin-DelaCruz et al. 2022, Rodriguez-
695 Caton, et al. 2021). Although the RW-precipitation correlations were robust, our results suggest that this *P. pepei* treeline is
696 likely more affected by temperature-related moisture stress changes (Fig. A4), as would be expected particularly at treeline
697 (Fritts, 1976). A pronounced decline in radial growth since 1997 (Fig. 2A) was observed at the same time this region has
698 endured warmer and drier austral summers (~November-March) in recent decades (Figs. A4, A5). The Keara treeline also
699 revealed an imprint of extreme ENSO-related drought events in *P. pepei* growth rings.

Formatted: Border: Top: (No border), Bottom: (No border),
Left: (No border), Right: (No border), Between : (No border)

Formatted: Font color: Text 1

Formatted: Font color: Text 1

Formatted: Border: Top: (No border), Bottom: (No border),
Left: (No border), Right: (No border), Between : (No border)

Hot-drought and dry conditions related to DJF-El Niño events years had a significant and negative impact on radial growth of *P. pepei* at our study site. Although La Niña SEA were inconclusive, the lagged negative effect ($t-3$) may be related to the occurrence of El Niño events in years after La Niña. DJF anomalies were (Fig. 6C). Although similar RW responses to large-scale drought DJF ENSO events were selected for analyses because they occur during mature phase of the summer monsoon (70% of annual rainfall), but the use of annual (instead of seasonal) events may show larger impacts on RW.

Future advances of this treeline towards higher elevations (Fig. 1C) are unlikely due to local geomorphologic constraints (Macias-Fauria and Johnson, 2013) and thermal niches that are required for subalpine recruitment (impacts of annual or broader seasonal ENSO extremes may be more informative due to the sensitivity of RW to cumulative climate conditions (e.g. seasonal correlations Fig. A4). Overall local and regional climate-growth analyses suggest this treeline is primarily limited by temperature-driven moisture stress during the peak wet season (~November-March Figs 3.4, A3, A4). Kessler et al., 2014; Körner and Hoch, 2023). As mentioned in the Introduction, *Polylepis pepei* in the tropical Andes is adapted to cold soil temperatures (3–5°C). Although the future spatial extent of the *P. pepei* forest under warming is uncertain, our study provides insight into the limiting factors to radial growth at a tropical Andean treeline in Bolivia since 1960. In the following sections we discuss potential local environmental and climate variables both site-level and large-scale hydroclimate conditions that may contribute to have contributed to the growth decline of treeline *P. pepei* tree-ring variability in Keara since the 1960s.

4.2. Changes in temperatures Local temperature and humidity changes at the *P. pepei* treeline in Bolivia

Increases in minimum temperature (T_{min}) may be reducing moisture availability in high-elevation Andean tropical sites. Hourly forests. The mean diurnal temperature range near Keara has significantly and negatively declined since 1960, signifying that the rate of minimum temperature increase has surpassed that of maximum temperature (Fig. A5. CRU TS 4.08 ;1901-2015). Daily climate data recorded by data loggers at our within the *P. pepei* site (Fig. A3) showed that the period September indicated the 2021-May-2022 had wet season was significantly warmer T_{min} and lower relative humidity (RH) in comparison to the period and drier than in 2011-2014 ($p < 0.0001$ October-April). This decrease in RH relative humidity alongside an increase in temperature minimum temperatures suggests that the capacity of air to hold moisture has outpaced the actual moisture content, making the air drier despite higher temperatures. Although these results the data logger records cover a short time window, they provide in situ evidence of, high-resolution data over a 10-year period in Keara, and thus they are useful to confirm: i.) the warming and drying trends observed in the long-term climate data of this site (Fig. A4). DTR variability (i.e. difference between T_{max} and T_{min}) near Keara in Fig. A5 depicts a significant negative trend in this region since 1960, which means the rate of increase for minimum temperatures has surpassed that of maximum temperature. Even though warmer temperatures increase the capacity of the air to hold more water vapor (i.e., the Clausius-Clapeyron relation), if the moisture supply does not increase proportionally, humidity will decrease (Fig. 4, A5), and ii.) that the increase in minimum temperatures coincided with a decrease in humidity at this site (Fig. A6).

Formatted: Border: Top: (No border), Bottom: (No border), Left: (No border), Right: (No border), Between : (No border)

Formatted: Font color: Text 1

Formatted: Border: Top: (No border), Bottom: (No border), Left: (No border), Right: (No border), Between : (No border)

735 *P. pepei* had significant negative correlations with increasing RW was significantly and negatively impacted by lower wet-
736 season precipitation and higher minimum temperatures on the local and spatial scale (Figs. 3 and 4 even after linear trends in
737 climate were removed (Fig. A4; residual correlations). Minimum temperatures influence convection, as rainfall in the Andes-
738 Amazon ecotone largely occurs in the afternoon/night when radiative cooling drives cold air downslope and converges with
739 rising warm moist air from the tropical lowlands (Garreaud, 1999; 2009; Junquas et al., 2018; Romatschke and Houze, 2010);
740 Rosales et al., 2022). Known as 'orographic precipitation', this process is key for rainfall distribution across elevations in the
741 Andean foothills like our site (Arias et al., 2021; Chavez and Takahashi, 2017). According to the hourly in situ data loggers in
742 Keara, daily RH peaked at 3:00 P.M. on average, likely reflecting afternoon cloud formation at this site. In the region of the
743 MNP, maximum precipitation occurred totals occur between 1000-1300 m.a.s.l., with a sharp decrease in moisture distribution
744 towards higher elevations → transport above 3000 m.a.s.l. (Chavez and Takahashi, 2017). If minimum temperatures increase,
745 the radiative cooling effect is weaker weakens, which may result in warm, moist air converging at lower elevations, (e.g. below
746 our treeline-*P. pepei* site-) (Romatschke and Houze, 2010). The hourly meteorological data between September-May in terms
747 of tree-growth in 2011-14 and 2022-23 shows that RH peaks at 3:00 P.M. in Keara on average, suggesting afternoon cloud
748 formation. It's this area, one interesting to note observation is the declining *P. pepei* RW trends observed in *P. pepei* (>3800 at
749 the MNP treeline (above 4000 m.a.s.l.)) diverge from the increasing RW trends observed in lower-elevation humid forests
750 from MNP since in the 1980s MNP (e.g. *Juglans boliviana* ~1300 m.a.s.l.) (Oelkers et al. 2023). It is possible that the increase
751 in T_{min} since the late 20th century (Fig. A5) may have contributed to reduced orographic convection and moisture availability,
752 thus potentially limiting the growth of *P. pepei*. Future research needs to be conducted on horizontal moisture transport in the
753 Andes-Amazon and the diverging trends in growth between the lower-Amazon and treeline forests.

754
755 One possible explanation for this pattern is that warmer minimum temperatures alter the local balance between temperature,
756 humidity, and upslope moisture transport in the Andes-Amazon ecotone. Because precipitation at these elevations depends
757 strongly on orographic processes and on the interaction between moist lowland air and cooler mountain conditions, weaker
758 nighttime cooling could reduce the efficiency of moisture convergence at the elevation of the treeline. We cannot demonstrate
759 that mechanism directly here, but the observed increase in minimum temperature, decline in DTR, and reduction in relative
760 humidity in Keara are all consistent with a shift toward locally dry conditions that may limit *P. pepei* growth (Figs 4, A5, A6).
761 In this sense, the results point to moisture stress amplified by warming, rather than temperature alone, as the most plausible
762 explanation for the long-term decline in ring width at the MNP treeline. Future research needs to be conducted on elevational
763 moisture transport in the Andes-Amazon and these diverging tree growth trends observed within the MNP.

764
765 Besides inhibiting moisture convergence and transport from lower elevations, warmer minimum temperatures could also affect
766 the tree water-balance in Keara by increasing transpiration and respiration rates (Sierra et al., 2022). A global analysis of
767 tropical tree longevity using tree-ring and other data found that tree mortality is increasing in all tropical biomes due to heat-
768 related water stress and increased evaporative demand at the leaf level (Locosselli et al., 2020). From an ecophysiological

Formatted: Border: Top: (No border), Bottom: (No border),
Left: (No border), Right: (No border), Between : (No border)

Formatted: Border: Top: (No border), Bottom: (No border),
Left: (No border), Right: (No border), Between : (No border)

769 perspective, respiration rates increase with ~~rising warmer~~ temperatures ~~and~~. Excessive warming at night (i.e. increased Tmin)
770 without ~~the process of~~ photosynthesis ~~occurring at night~~. This in turn ~~increases~~ may increase the amount of ~~tree-level~~ carbon
771 (~~respiration~~) and ~~soil-water~~ content released ~~from the trees~~ to the atmosphere. (Körner et al. 2012). Temperature and
772 precipitation near the *P. pepei* site are inversely correlated during ~~the extended peak~~ wet season (~~October-April~~ (~November-
773 March, $p < 0.05$). ~~If~~ Thus, if there is less cloud cover (and ~~rainfall~~ precipitation), there is higher solar irradiance and temperatures,
774 which may limit the photosynthetic capacity of ~~trees especially in~~ tropical ~~trees at higher elevations~~ moist treelines (García-
775 Núñez et al., 2004; Hoch and Körner, 2005; Jaramillo, 2015). ~~The current year positive relationship between RW and FMA~~
776 ~~Tmax (Fig. 3C, Fig. 4B)~~, may also highlight the ecophysiological link between tree ring size (i.e. xylogenesis) and cooler
777 trends in Tmax at the end of the wet season between 1960-2015 (see discussion in Rodríguez-Catón et al. 2021). Although it
778 is possible that the timing of the mechanisms controlling primary (photosynthesis) and secondary growth (wood formation)
779 may not occur at the same time, the RW-climate correlations show there is less radial growth if is warmer and drier than when
780 it is cooler and wetter (Figs. 3, A4). Further research must be conducted to determine the phenology and physiological response
781 of *P. pepei* to micro-climate conditions such as a reduction in orographic precipitation at ~~at~~ this treeline or low to diurnal and
782 seasonal changes in orography and soil-water availability.

783
784 The positive relationship between *P. pepei* and February-May mean and max temperatures may demonstrate ecophysiological
785 link between tree-ring size (i.e. xylogenesis) and cooling observed at the end of the wet season (lag=0; FMAM Tmax Figs.
786 3BD, A3BD). Although it is possible the mechanisms controlling primary and secondary growth may not occur at the same
787 time (i.e. photosynthesis vs. wood formation), the RW-climate correlations indicate growth rings are smaller when there are
788 cooler conditions in late austral summer (or vice versa; Figs. 3, 4). It is interesting to note that an extreme cold period observed
789 near Keara during the late 1950s corresponds with a growth suppression observed in raw, standard and residual *P. pepei* RW
790 chronologies, emphasizing the coupled relationship between RW and mean and maximum temperatures during this period
791 (Figs. A5B, C and 2A, C). The exact growing season for *P. pepei* in Keara estimated to be during the wet season (~ October-
792 April), but the phenology of *P. pepei* in the MNP and elsewhere is largely unknown. The use of point-dendrometer bands that
793 record high resolution variations of stem circumference may reduce uncertainty regarding the onset and cessation of tree-
794 growth during the hydrological year and its relationship temperature variability between February to May.

796 4.3. Large-scale climate variability impacting tree growth in tropical Andean treelines

797 ~~The~~ In addition to site-level conditions at this treeline, the recent decline in ~~radial~~ annual growth may ~~be~~ also ~~influeneced by~~ ~~be~~
798 ~~linked to~~ broader scale hydroclimate ~~ehanges~~ patterns observed in tropical south America. In the central Andes treeline,
799 ($>17^{\circ}\text{S}$; 4657-4800 m.a.s.l.). ~~Negative~~ negative RW trends in *P. tarapacana* since the 1970s were attributed to increasing
800 drought conditions in southern Peru and northern Chile ~~since the 1970s~~. ($>17^{\circ}\text{S}$; 4657-4800 m.a.s.l.) (Morales et al. (2023)
801 developed a NDJ precipitation reconstruction from these trees and discovered that a drying trend since 1997 was unprecedented
802 in the 389 yr reconstruction. Although 1997 was identified as a changepoint in the raw ring width data of *P. pepei*, our site is

Formatted: Border: Top: (No border), Bottom: (No border),
Left: (No border), Right: (No border), Between : (No border)

Formatted: Border: Top: (No border), Bottom: (No border),
Left: (No border), Right: (No border), Between : (No border)

803 in the Amazon basin, a much more humid environment than the *P. tarapacana* in Morales et al. (2023). Nonetheless the shared
804 timing of growth decline in these high-Andes forests is interesting.

805
806). Increasing drought frequency in the tropical Andes and southern Amazon Basin ($> -15^{\circ}\text{S}$) has been linked to delayed wet
807 season onset (Espinoza et al., 2016; Fu et al., 2013; Marengo et al., 2011). One possible explanation is ~~anthat the~~ intensification
808 of the atmospheric Hadley ~~circulation, related to~~ Circulation during the 20th century, driven by warming SST in the ~~(northern)~~
809 tropical Atlantic Ocean, which interrupts upward flows from the Amazon, has led to the Andes a weakening of zonal moisture
810 transport and in increase in subsidence during ~~thetransitional~~ dry-to-wet period seasons in the central Andes (Beveridge et al.,
811 2024; Espinoza et al., 2021, 2019; Sierra et al. 2022; Yoon and Zeng, 2010). In particular, ~~Ronehail et al. (2018) and Espinoza~~
812 ~~et al. (2019) found a significant increase in dry-day frequency between September–November in Bolivia and Peru which marks~~
813 ~~a delay in the timing of austral spring rainfall.~~ Additionally, an observed weakening of upper-level easterlies winds from the
814 Amazon to the Andes (Segura et al. 2022). In that context, the decline observed in *P. pepeii* may have contributed to reduced
815 moisture transport potentially affecting tropical ~~bc part of a wider pattern of increasing hydroclimatic stress at high elevations~~
816 in the tropical Andes. At the same time, the Keara site differs from drier Polylepis treelines like *P. pepeii* in Keara such as *P.*
817 *tarapacana* (Morales et al. 2023:), so annual growth-comparisons should be interpreted cautiously.

818
819 In contrast to a drier start to the wet-season, a recent increase in precipitation at the end of the wet season ~~< 2000 m.a.s.l.~~ has
820 been observed in lowland regions ~~efbelow 2000 m.a.s.l. in~~ the northern Andes and Amazon and Andes-Amazon Basin (Arias
821 et al., 2021; Espinoza et al., 2021, 2019; Malhi et al., 2008; Zanin and Satyamurty, 2020). These studies argue that ~~the~~ warming
822 of the Atlantic Ocean, land-surface changes in the Amazon, and wind anomalies are the primary factors contributing to changes
823 in ~~circulation and~~ specific humidity in tropical south America overall ~~(particularly between March–May; see references in~~
824 ~~(Beveridge et al., 2024)). Within Bolivia, contrasting trends in~~ Contrasting precipitation and tree-growth trends have been
825 observed ~~between lowat various latitudes and highland elevation forests. Tree elevations within Bolivia as well. tree-ring~~
826 oxygen isotopes ($\delta^{18}\text{O}(\text{d}^{18}\text{O})$) from ~~C-Cedrela odorata~~ in the lowland Bolivian Amazon (10°S , 66°W ; 106 m.a.s.l.)
827 reflected an increase in November–March precipitation ~~(and decrease in $\delta^{18}\text{O}$)~~ between 1980–2010 ~~-(10°S, 66°W; 106~~
828 ~~m.a.s.l.)~~ Baker et al., 2016; Cintra et al., 2025), while treeline *P. tarapacana*, ~~ind¹⁸O from~~ the Bolivian Altiplano (22.3°S ;
829 67.23°W ; ~4600 m.a.s.l.) recorded a pronounced dry period for decrease in December–March precipitation between 1992–
830 2012 (22.3°S , 67.23°W ; ~4600 m.a.s.l.; Baker et al., 2016; Cintra et al., 2025; Rodriguez-Caton et al., 2024). ~~Despite the fact~~
831 ~~that~~ Even though these hydroclimate trends are complex and spatially variable, having *in situ* high-resolution climate proxies
832 at the Andes-Amazon treeline such as ~~this~~ *P. pepeii* may be useful in understanding long-term changes in orography.

833
834 Overall, growth variability at this *P. pepeii* treeline ~~in-is modulated by temperatures and moisture available at the site, which~~
835 ~~may be influence by small-scale climate dynamics driven by orography, but may also reflect broader hydroclimatic changes~~
836 across the tropical Andes- and adjacent Amazon ~~here may be related~~ basin mentioned above. Rather than implying a shared

Formatted: Border: Top: (No border), Bottom: (No border), Left: (No border), Right: (No border), Between : (No border)

Formatted: Font color: Text 1

Formatted: Font color: Text 1

Formatted: Font: Italic, Font color: Text 1

Formatted: Font color: Text 1

Formatted: Font color: Text 1

Formatted: Font color: Text 1

Formatted: Border: Top: (No border), Bottom: (No border), Left: (No border), Right: (No border), Between : (No border)

mechanism across all Andean treelines, our results suggest that distinct *Polylepis* treelines may be responding to temperature-driven moisture trends observed at local and a common regional scales. This study herein has demonstrated the dendroclimatic potential of this species at a trend toward warmer and, in some cases, effectively drier conditions during the peak wet-season near the Andes-Amazon treeline from the most biodiverse region of the world (MNP; Muller, 2017) and (~November-March). Overall, this newly-generated record has provided insight into the in situ evidence of a long-term, and negative growth response of a tropical forest in South America under a warming environment. treeline to increased temperature trends in Northwestern Bolivia between 1960-2015 (14°S, 4400 m.a.s.l.).

5 Conclusions

We reported a significant decline in radial growth in *Polylepis pepeii* at a tropical *P. pepeii* treeline in Keara, Bolivia, at the edges of the Andes-southwestern Amazon high-elevation forests. Here, growth decreases Basin (~4400 m a.s.l.). Our results indicate that this decline is associated with warmer increasingly warm and drier dry conditions in since the 1960s, particularly through reduced precipitation and higher minimum temperatures during the prior-year wet season, and there is an adverse influence of temperatures, in particular T_{min}, on growth. Higher T_{min} weakens preceding ring formation. Together, these changes suggest increasing moisture stress at the site. Rising minimum temperatures, especially when not matched by equivalent increases in maximum temperatures, may also reduce moisture availability by lowering relative humidity, altering local moisture transport, and increasing nighttime convection that brings moisture from lower elevations to this site, and in general respiratory carbon losses. More broadly, warmer conditions increase are likely to enhance evaporative demands demand and cause water stresses further constrain tree growth. We also found a tendency for narrower growth-rings in the year following warm and dry El Niño events, while whereas the role influence of La Niña events was inconclusive. This remained less clear, suggesting an asymmetric influence of ENSO on tree growth warrants further investigations. Moving forward, since we found *P. pepeii* to develop annual rings effect that are climate sensitive, expanding deserves further study. Expanding the *P. pepeii* network in Keara would enable at Keara could provide the basis for the first tree-ring-based climate reconstructions of precipitation and temperature of the southwestern Amazon-Andes ecotone. This would be the first of its kind for northern Bolivia, extending the limited station records short instrumental record back to the mid-1800s. Our results nineteenth century. Overall, our findings provide new insights insight into the response vulnerability of a tropical treeline in an era of global treelines to ongoing warming, increasing climate extremes, and human activities hydroclimatic change, and support they highlight the value of *P. pepeii* for future dendrochronological and ecophysiological research of *P. pepeii* in South America. We recommend pursuing research that in the tropical Andes. Future work should thus focus on quantifying leaf respiration and temperature response, temperature sensitivity, and the timing of wood formation using ecophysiological measurements and point dendrometers, to better understand the ecophysiology of mechanisms linking climate change and growth decline in this tropical treeline species in Bolivia.

Formatted: Border: Top: (No border), Bottom: (No border), Left: (No border), Right: (No border), Between : (No border)

Formatted: Border: Top: (No border), Bottom: (No border), Left: (No border), Right: (No border), Between : (No border)

869 **Author contribution**

870 Co-authors LAH, DRC, MRC, MEF, RO, ET, AF collected tree samples in Keara. CM and AF organized field campaigns and
871 provided essential information regarding Madid National Park. RDD and LAH assisted in initial experimental design and
872 editing. Tree-ring dating, measuring, and analyses was conducted by corresponding other RO. HTTN, aided in correlation
873 analyses and concept. APS assisted in wood anatomical methods. Editorial review provided by all co-authors. Site images for
874 [FigFigs. 1 and A2](#) were taken by RO.

875 **Competing interests**

876 The authors declare that they have no conflict of interest

877 **Acknowledgements**

878 This work was made possible by the following funding sources from the U.S. National Science Foundation: AGS-1702789,
879 AGS-1903687, AGS-2303524, and OISE-1743738. We acknowledge the NSF AGS-1903690-[grant at UC Irvine-KCCAMS](#)
880 [facility](#)-for seven radiocarbon measurements. E.T. received funding from the Comunidad de Madrid program Atracción
881 Talento “César Nombela” grant number 2023-T1/ECO-29118. [We thank Marco Tedesco’s Lab at LDEO for making the Echo](#)
882 [microscope camera available for the anatomical images](#). This work is dedicated to Renaud, his family and the community of
883 Keara for their hospitality, knowledge, and assistance in the field. Special thanks the Nacional Herbario in La Paz, including
884 Alfredo Fuentes and Freddy “Zen” Ruiz, for their guidance during the 2012 and 2019, 2023 Bolivian field campaigns.

885 **Data Availability**

886 The *Polylepis pepei* RW chronology from Keara will be made publicly available on the NOAA International Tree-ring
887 Database.

888

889

890

891

892

893

894

Formatted: Border: Top: (No border), Bottom: (No border),
Left: (No border), Right: (No border), Between : (No border)

Formatted: Border: Top: (No border), Bottom: (No border),
Left: (No border), Right: (No border), Between : (No border)

895
896
897
898
899
900
901
902
903
904
905
906

Appendix A

907
908

<u>El Niño DJF</u>	<u>La Niña DJF</u>
<u>1983</u>	<u>1974</u>
<u>1998</u>	<u>1917</u>
<u>1973</u>	<u>1956</u>
<u>1931</u>	<u>1976</u>
<u>1992</u>	<u>2011</u>
<u>1966</u>	<u>1989</u>
<u>1919</u>	<u>1910</u>
<u>1926</u>	<u>1971</u>
<u>1958</u>	<u>1951</u>
<u>1897</u>	<u>2000</u>
<u>2010</u>	<u>1918</u>

Formatted: Border: Top: (No border), Bottom: (No border), Left: (No border), Right: (No border), Between : (No border)

Formatted: Font color: Text 1

Formatted: Border: Top: (No border), Bottom: (No border), Left: (No border), Right: (No border), Between : (No border)

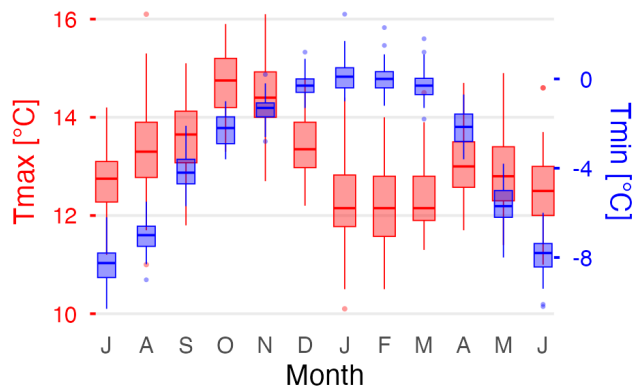
<u>1987</u>	<u>2008</u>
<u>1942</u>	<u>1943</u>

Table A1. NOAA-PSL list of 26 top ranked DJF-ENSO events (13 each) which were selected for SEA analyses of *P. pepel* RW. The years provided for the DJF seasons are centered on January. The remaining 22 top ranked events (48 total) are available on the website (https://psl.noaa.gov/enso/past_events.html).

Formatted: Border: Top: (No border), Bottom: (No border), Left: (No border), Right: (No border), Between : (No border)

Formatted: Border: Top: (No border), Bottom: (No border), Left: (No border), Right: (No border), Between : (No border)

A
Diurnal temperature range 1960–2015



B

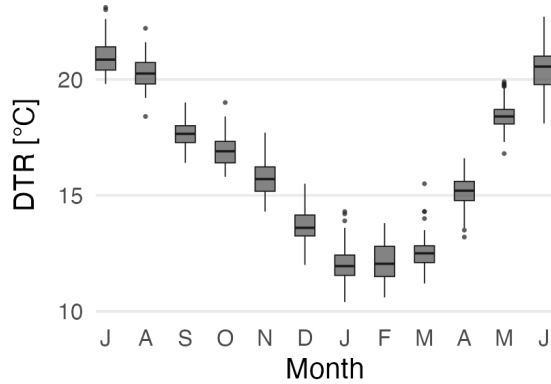


Figure A1: (A) Boxplots of the mean monthly distribution of maximum and minimum temperatures and (B) the diurnal temperature range (grey:DTR) for the study region between 1960-2015 using the nearest CRU 4.08 grid point data (14.75,69.25). Boxplots include the temperature median (horizontal line), 1.5x the inter-quartile range (whiskers), and outliers (colored dots).

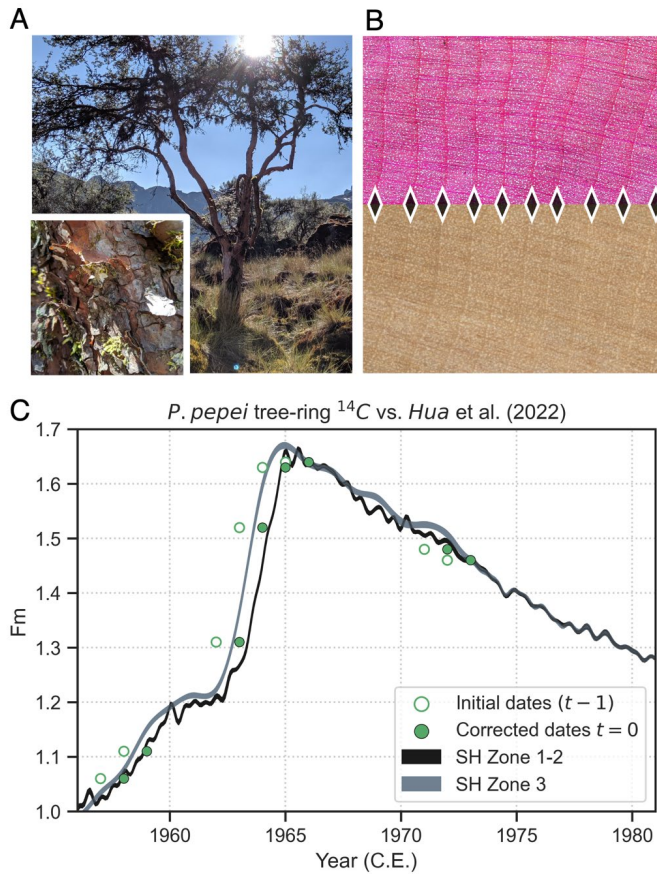
919

920 **Appendix A2. Photo of *Polylepis pepeii*, Wood anatomy and Radiocarbon Analyses**

921 At early stages of RW chronology development for the *Polylepis pepeii* network, initial radiocarbon results (Fig. A2.C) showed
922 that ^{14}C measurements of SP20X were offset by 1 year in relation to the SH Zone ^{14}C curves. In the original *P. pepeii* RW
923 timeseries generated with material collected in October 2012, the first ring behind the bar was not measured as it was
924 considered an incomplete growth year. Upon a recent inspection of these samples, we observed that the final ring behind the
925 bark did not always correspond to a partial ring as some trees had not yet started wood formation for the 2012 growth year (at
926 least for the side of the stem where the core was sampled). Therefore, the calendar year assigned to the last complete ring for
927 the KEPP RW samples was corrected to 2011. This date-adjustment on the samples from the 2012 campaign was confirmed
928 after cross-dating RW from additional living trees collected in 2019 from the Waca-cocha closed-canopy forest. The final RW
929 chronology shown included 31 trees from 2019 (combined mean correlation, $r= 0.50$). In summary, the traditional
930 dendrochronological crossdating techniques of RW measurements, wood anatomical cuts, and radiocarbon results confirmed
931 *P. pepeii* in Keara formed annual rings.

Formatted: Border: Top: (No border), Bottom: (No border),
Left: (No border), Right: (No border), Between : (No border)

Formatted: Border: Top: (No border), Bottom: (No border),
Left: (No border), Right: (No border), Between : (No border)

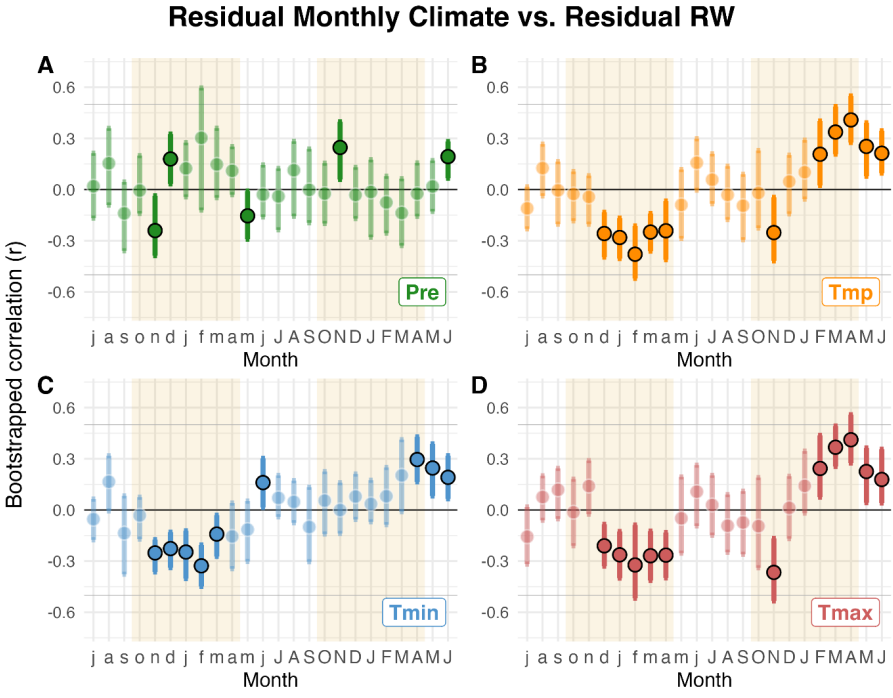


932 **Figure A2. (A) Photo of a *P. pepei* tree in Keara during the dry season in July 2019. The trees have evergreen foliage,**
 933 **and can appear shrublike, with twisted, and at times multiple, stems. The bark consists of thick layers of compressed**
 934 **flakes that are red and brown in color. (B) *P. pepei* wood anatomy for a histological slice (40X magnification Echo**
 935 **microscope camera) and scanned image of a tree-core (3200 dpi). The direction of radial growth is from left to right**
 936 **(pith to bark) while diamond shapes indicate the latewood/earlywood boundary between annua tree-rings. *P. pepei***
 937 **tree rings feature large, uniformly distributed vessels in the earlywood while the latewood includes both solitary**
 938 **vessels and thicker, fiber-like tracheid cells. The vessel lumen area in the latewood appears to taper tangentially in**
 939 **size before each subsequent growth-ring boundary. (C) Radiocarbon measurements (green circles) from the alpha-**
 940 **cellulose of selected rings in a cross-section is plotted with the Hua et al. (2022) reference curves SH Zone 1-2 and SH**
 941 **Zone 3.**
 942
 943

Formatted: Border: Top: (No border), Bottom: (No border), Left: (No border), Right: (No border), Between : (No border)

Formatted: Border: Top: (No border), Bottom: (No border), Left: (No border), Right: (No border), Between : (No border)

Formatted: Border: Top: (No border), Bottom: (No border), Left: (No border), Right: (No border), Between : (No border)



944

945

946

947

948

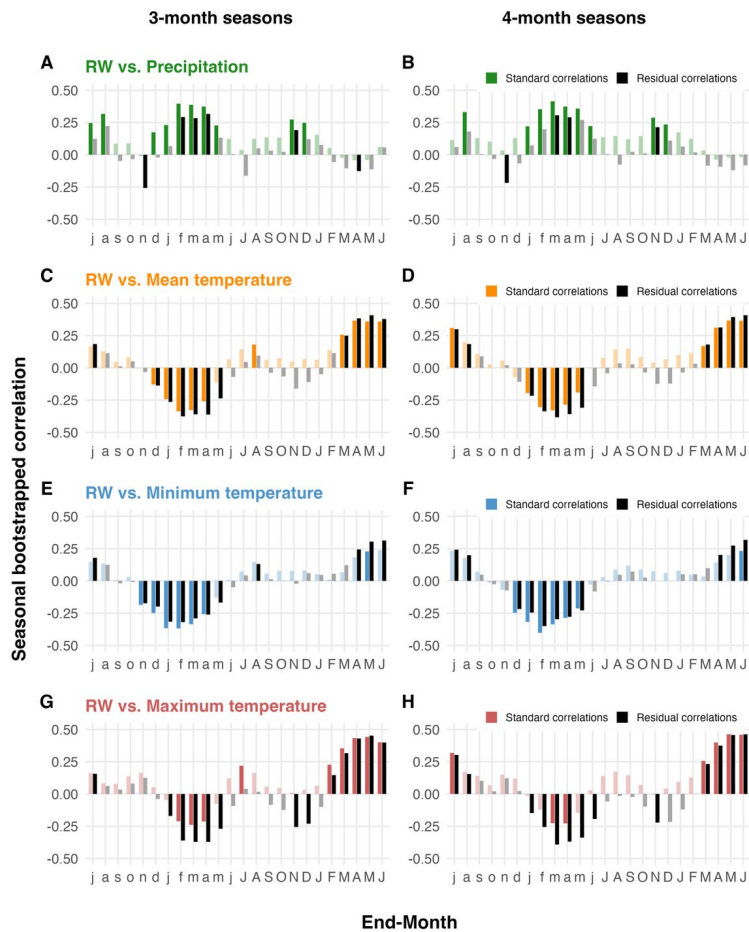
949

950

951

Figure A3. Residual *P. pepei* RW correlations with Residual monthly climate data 1960-2015. The residuals from a linear regression were applied to the local monthly precipitation (A), and mean, minimum, and maximum temperature series for the site (B-D) to evaluate the interannual relationships between annual RW and monthly climate variables. Lowercase letters on the x-axis represent prior-year climate (lag=1). Correlations are reported as the median r estimated using stationary bootstrapping. Significance was defined from 95% bootstrapped confidence intervals and are denoted in solid-colored circles outlined in black. Tan-shading represents the estimated 'wet-season' for the treeline site which extends between October-April for this period.

Formatted: Border: Top: (No border), Bottom: (No border), Left: (No border), Right: (No border), Between : (No border)

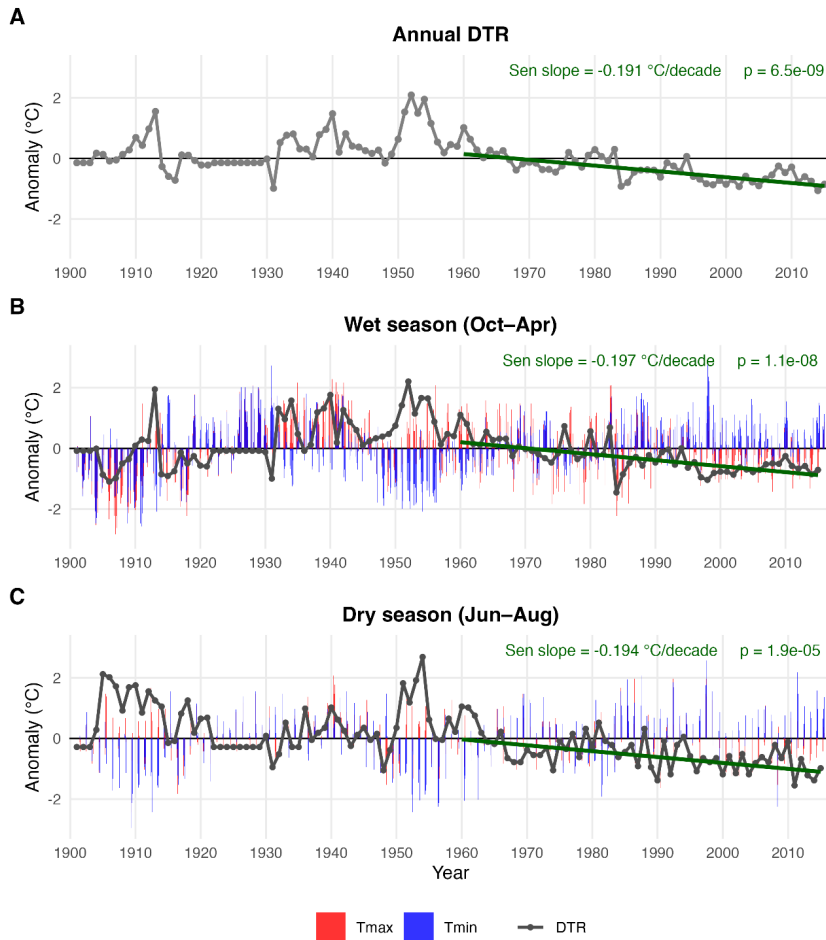


952
 953 **Figure A4. Running seasonal climate correlations with *P. pepei* RW for 3-month (left column) and 4-month (right**
 954 **column) seasonal averages using local temperature and precipitation data (1960-2015). ‘Residual correlations’ are**
 955 **represented as black bars (i.e. detrended climate vs. residual RW), while colored bars represent ‘standard correlations’**
 956 **(i.e. mean climate vs. standard RW). The x-axis represents the ‘end-month’ of the season, for example, lowercase ‘f’ in**
 957 **panel (A) represents correlations between RW and prior-year December-February precipitation (lag=1). Significance**
 958 **was inferred from 95% bootstrapped confidence intervals. Non-significant seasonal correlations are faded, while**
 959 **significant correlations are solid-colored bars.**

Formatted: Border: Top: (No border), Bottom: (No border), Left: (No border), Right: (No border), Between: (No border)

Formatted: Border: Top: (No border), Bottom: (No border), Left: (No border), Right: (No border), Between: (No border)

1901–2015 Temperature anomalies near the Keara treeline



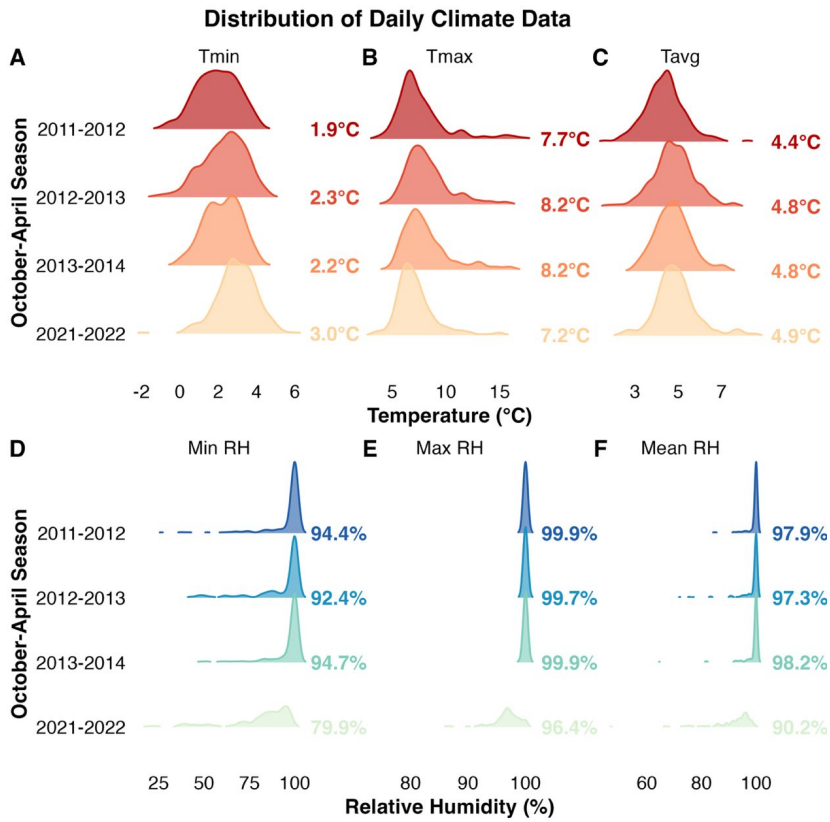
960
961 **Figure A5. Long-term temperature anomalies for the Keara site (1901-2015). The grey timeseries represents annual**
962 **(A) and seasonal (B-C) diurnal temperature range for the nearest gridpoint from CRU TS 4.08. 1901 is the earliest year**
963 **of available data for CRU. Linear trends in DTR anomalies were estimated using Sen’s slope. The significance of the**
964 **1960-2015 trend was evaluated using a two-tailed Mann-Kendall test. The mean slope is reported as the average change**
965 **in DTR per decade (°C). Seasonal anomalies for Tmax (red) and Tmin (blue) are represented as vertical bars for the**
966 **1901-2015 period (B-C).**

Formatted: Border: Top: (No border), Bottom: (No border), Left: (No border), Right: (No border), Between : (No border)

Formatted: Border: Top: (No border), Bottom: (No border), Left: (No border), Right: (No border), Between : (No border)

967
968

Formatted: Border: Top: (No border), Bottom: (No border), Left: (No border), Right: (No border), Between : (No border)



969
970
971
972
973
974
975

Figure A6. Ridgeline distributions of daily temperature and relative humidity between October–April for the 2011–2012, 2012–2013, 2013–2014, and 2021–2022 seasons at the site. This data was resampled from hourly measurements recorded *in situ* from dataloggers installed near the Keara open-canopy site in 2011 (see section 2.1). The top row (A–C) represents daily minimum (Tmin), maximum (Tmax), and mean (Tavg) temperature. The bottom row (D–F) displays minimum, maximum, and mean relative humidity (RH; bottom row). Colored ridges represent daily observations within each season, and bold values at the right margin indicate seasonal means for each year.

Formatted: Border: Top: (No border), Bottom: (No border), Left: (No border), Right: (No border), Between : (No border)

976

References

- 977 Argollo, J., Soliz, C., Villalba, R., 2004. Potencialidad dendrocronológica de *Polylepis tarapacana* en los Andes Centrales de
 978 Bolivia. *Ecol. En Bolív.* 39, 5–24.
- 979 Büntgen, U., Wacker, L., Galván, J.D., Arnold, S., Arseneault, D., Baillie, M., Beer, J., Bernabei, M., Bleicher, N., Boswijk,
 980 G., Bräuning, A., Carrer, M., Ljungqvist, F.C., Cherubini, P., Christl, M., Christie, D.A., Clark, P.W., Cook, E.R.,
 981 D'Arrigo, R., Davi, N., Eggertsson, O., Esper, J., Fowler, A.M., Gedalof, Z., Gennaretti, F., Griesinger, J., Grissino-
 982 Mayer, H., Grudd, H., Gunnarson, B.E., Hantemirov, R., Herzig, F., Hessler, A., Heussner, K.-U., Jull, A.J.T.,
 983 Kukarskih, V., Kirdyanov, A., Kolář, T., Krusic, P.J., Kynel, T., Lara, A., LeQuesne, C., Linderholm, H.W., Loader,
 984 N.J., Luckman, B., Miyake, F., Myglan, V.S., Nicolussi, K., Oppenheimer, C., Palmer, J., Panyushkina, I., Pederson,
 985 N., Rybníček, M., Schweingruber, F.H., Seim, A., Sigl, M., Churakova (Sidorova), O., Speer, J.H., Synal, H. A.,
 986 Tegel, W., Treydte, K., Villalba, R., Wiles, G., Wilson, R., Winship, L.J., Wunder, J., Yang, B., Young, G.H.F., 2018.
 987 Tree rings reveal globally coherent signature of cosmogenic radiocarbon events in 774 and 993 CE. *Nat. Commun.*
 988 9, 3605. <https://doi.org/10.1038/s41467-018-06036-0>
- 989 Crispin-DelaCruz, D.B., Morales, Mariano.S., Andreu-Hayles, Laia, Christie, Duncan.A., Guerra, A., Requena-Rejas,
 990 Edilson.J., 2022. High ENSO sensitivity in tree rings from a northern population of *Polylepis tarapacana* in the
 991 Peruvian Andes. *Dendrochronologia* 71, 125902. <https://doi.org/10.1016/j.dendro.2021.125902>
- 992 D'Arrigo, R., Jacoby, G., Free, M., Robock, A., 1999. Northern Hemisphere Temperature Variability for the Past Three
 993 Centuries: Tree-Ring and Model Estimates. *Clim. Change* 42, 663–675. <https://doi.org/10.1023/A:1005471918574>
- 994 Farfan-Rios, W., Feeley, K.J., Myers, J.A., Tello, S., Sallo-Bravo, J., Malhi, Y., Phillips, O.L., Baker, T.R., Nina-Quispe, A.,
 995 Garcia-Cabrera, K., 2025. Amazonian and Andean tree communities are not tracking current climate warming. *Proc.*
 996 *Natl. Acad. Sci.* 122, e2425619122.
- 997 MacDonald, G.-m., Kremenetski, K. v., Beilman, D. w., 2007. Climate change and the northern Russian tree-line zone. *Philos.*
 998 *Trans. R. Soc. B Biol. Sci.* 363, 2283–2299. <https://doi.org/10.1098/rstb.2007.2200>
- 999 Politis, D.N., Romano, J.P., 1994. The Stationary Bootstrap. *J. Am. Stat. Assoc.* 89, 1303–1313.
 1000 <https://doi.org/10.1080/01621459.1994.10476870>
- 1001 Rodriguez-Caton, M., Andreu-Hayles, L., Daux, V., Vuille, M., Varuolo-Clarke, A.M., Oelkers, R., Christie, D.A., D'Arrigo,
 1002 R., Morales, M.S., Palat-Rao, M., Srur, A.M., Vimieux, F., Villalba, R., 2022. Hydroclimate and ENSO Variability
 1003 Recorded by Oxygen Isotopes From Tree Rings in the South American Altiplano. *Geophys. Res. Lett.* 49,
 1004 <https://doi.org/10.1029/2021GL095883>
- 1005 Rodriguez-Caton, M., Andreu-Hayles, L., Morales, M.S., Daux, V., Christie, D.A., Coopman, R.E., Alvarez, C., Rao, M.P.,
 1006 Aliste, D., Flores, F., Villalba, R., 2021. Different climate sensitivity for radial growth, but uniform for tree-ring
 1007 stable isotopes along an aridity gradient in *Polylepis tarapacana*, the world's highest elevation tree species. *Tree*
 1008 *Physiol.* 41, 1353–1371. <https://doi.org/10.1093/treephys/tpab021>
- 1009 Rodriguez-Caton, M., Morales, M.S., Rao, M.P., Nixon, T., Vuille, M., Rivera, J.A., Oelkers, R., Christie, D.A., Varuolo-
 1010 Clarke, A.M., Ferrero, M.E., Magney, T., Daux, V., Villalba, R., Andreu-Hayles, L., 2024. A 300-year tree-ring
 1011 $\delta^{18}\text{O}$ -based precipitation reconstruction for the South American Altiplano highlights decadal-hydroclimate
 1012 teleconnections. *Commun. Earth Environ.* 5, 1–13. <https://doi.org/10.1038/s43247-024-01385-9>
- 1013 Akaike, H., 1974. A new look at the statistical model identification. *IEEE Trans. Autom. Control* 19, 716–723.
- 1014 Álvarez, C., Veblen, T.T., Christie, D.A., González-Reyes, Á., 2015. Relationships between climate variability and radial
 1015 growth of *Nothofagus pumilio* near altitudinal treeline in the Andes of northern Patagonia, Chile. *For. Ecol. Manag.*
 1016 342, 112–121. <https://doi.org/10.1016/j.foreco.2015.01.018>
- 1017 Alvites, C., Battipaglia, G., Santopuoli, G., Hampel, H., Vázquez, R.F., Matteucci, G., Tognetti, R., 2019. Dendrochronological
 1018 analysis and growth patterns of *Polylepis reticulata* (Rosaceae) in the Ecuadorian Andes. *IAWA J.* 40, 331-35.
 1019 <https://doi.org/10.1163/22941932-40190240>
- 1020 Andreu-Hayles, L., Tejedor, E., D'Arrigo, R., Locosselli, G.M., Rodríguez-Catón, M., Daux, V., Oelkers, R., Pacheco-Solana,
 1021 A., Paredes-Villanueva, K., Rodríguez-Morata, C., 2023. Dendrochronological advances in the tropical and
 1022 subtropical Americas: Research priorities and future directions. *Dendrochronologia* 81, 126124.
 1023 <https://doi.org/10.1016/j.dendro.2023.126124>

Formatted: Border: Top: (No border), Bottom: (No border),
Left: (No border), Right: (No border), Between : (No border)

Formatted: Font color: Black

Formatted: Border: Top: (No border), Bottom: (No border),
Left: (No border), Right: (No border), Between : (No border)

- 1024 [Argollo, J., Soliz, C., Villalba, R., 2004. Potencialidad dendrocronológica de *Polylepis tarapacana* en los Andes Centrales de](#)
1025 [Bolivia. *Ecol. En Bolív.* 39, 5–24.](#)
- 1026 Arias, P.A., Garreaud, R., Poveda, G., Espinoza, J.C., Molina-Carpio, J., Masiokas, M., Viale, M., Scaff, L., van Oevelen, P.J.,
1027 2021. Hydroclimate of the Andes Part II: Hydroclimate Variability and Sub-Continental Patterns. *Front. Earth Sci.* 8.
1028 <https://doi.org/10.3389/feart.2020.505467>
- 1029 Batllori, E., Gutiérrez, E., 2008. Regional tree line dynamics in response to global change in the Pyrenees. *J. Ecol.* 96, 1275–
1030 1288. <https://doi.org/10.1111/j.1365-2745.2008.01429.x>
- 1031 Beveridge, C.F., Espinoza, J.-C., Athayde, S., Correa, S.B., Couto, T.B.A., Heilpern, S.A., Jenkins, C.N., Piland, N.C.,
1032 Utsunomiya, R., Wongchuig, S., Anderson, E.P., 2024. The Andes–Amazon–Atlantic pathway: A foundational
1033 hydroclimate system for social–ecological system sustainability. *Proc. Natl. Acad. Sci.* 121, e2306229121.
1034 <https://doi.org/10.1073/pnas.2306229121>
- 1035 [Bunn, A.G., 2008. A dendrochronology program library in R \(dplR\). *Dendrochronologia* 26, 115–124.](#)
1036 <https://doi.org/10.1016/j.dendro.2008.01.002>
- 1037 Buras, A., 2017. A comment on the expressed population signal. *Dendrochronologia* 44, 130–132.
1038 <https://doi.org/10.1016/j.dendro.2017.03.005>
- 1039 [Büntgen, U., Wacker, L., Galván, J.D., Arnold, S., Arseneault, D., Baillie, M., Beer, J., Bernabei, M., Bleicher, N., Boswijk,](#)
1040 [G., Bräuning, A., Carrer, M., Ljungqvist, F.C., Cherubini, P., Christl, M., Christie, D.A., Clark, P.W., Cook, E.R.,](#)
1041 [D'Arrigo, R., Davi, N., Eggertsson, O., Esper, J., Fowler, A.M., Gedalof, Z., Gennaretti, F., Gießinger, J., Grissino-](#)
1042 [Mayer, H., Grudd, H., Gunnarson, B.E., Hantemirov, R., Herzog, F., Hessler, A., Heussner, K.-U., Jull, A.J.T.,](#)
1043 [Kukarskih, V., Kirilyanov, A., Kolář, T., Krusic, P.J., Kyncl, T., Lara, A., LeQuesne, C., Linderholm, H.W., Loader,](#)
1044 [N.J., Luckman, B., Miyake, F., Myglan, V.S., Nicolussi, K., Oppenheimer, C., Palmer, J., Panushkina, I., Pederson,](#)
1045 [N., Rybníček, M., Schweingruber, F.H., Seim, A., Sigl, M., Churakova \(Sidorova\), O., Speer, J.H., Sval, H.-A.,](#)
1046 [Tegel, W., Treydte, K., Villalba, R., Wiles, G., Wilson, R., Winship, L.J., Wunder, J., Yang, B., Young, G.H.F., 2018.](#)
1047 [Tree rings reveal globally coherent signature of cosmogenic radiocarbon events in 774 and 993 CE. *Nat. Commun.*](#)
1048 [9, 3605. <https://doi.org/10.1038/s41467-018-06036-0>](#)
- 1049 Camarero, J.J., Mendivelso, H.A., Sánchez-Salguero, R., 2020. How Past and Future Climate and Drought Drive Radial-
1050 Growth Variability of Three Tree Species in a Bolivian Tropical Dry Forest, in: Pompa-García, M., Camarero, J.J.
1051 (Eds.), *Latin American Dendroecology: Combining Tree-Ring Sciences and Ecology in a Megadiverse Territory*.
1052 Springer International Publishing, Cham, pp. 141–167. https://doi.org/10.1007/978-3-030-36930-9_7
- 1053 [Canty, A., Ripley, B., 2017. Package 'boot.' *Bootstrap Funct. CRAN R Proj.*](#)
- 1054 Chavez, S.P., Takahashi, K., 2017. Orographic rainfall hot spots in the Andes–Amazon transition according to the TRMM
1055 precipitation radar and in situ data. *J. Geophys. Res. Atmospheres* 122, 5870–5882.
1056 <https://doi.org/10.1002/2016JD026282>
- 1057 Cook, E.R., Briffa, K.R., Shiyatov, S., Mazepa, V., 1990. Tree-ring standardization and growth-trend estimation 104–123.
- 1058 Cook, E.R., Peters, K., 1981. The Smoothing Spline: A New Approach to Standardizing Forest Interior Tree-Ring Width Series
1059 for Dendroclimatic Studies.
- 1060 [Cook, E.R., Pederson, N., 2011. Uncertainty, Emergence, and Statistics in Dendrochronology. in: Hughes, M.K., Swetnam,](#)
1061 [T.W., Diaz, H.F. \(Eds.\), *Dendroclimatology: Progress and Prospects*. Springer Netherlands, Dordrecht, pp. 77–112.](#)
1062 https://doi.org/10.1007/978-1-4020-5725-0_4
- 1063 [Crispin-DelaCruz, D.B., Morales, Mariano S., Andreu-Hayles, Laia, Christie, Duncan A., Guerra, A., Requena-Rojas,](#)
1064 [Edilson J., 2022. High ENSO sensitivity in tree rings from a northern population of *Polylepis tarapacana* in the](#)
1065 [Peruvian Andes. *Dendrochronologia* 71, 125902. <https://doi.org/10.1016/j.dendro.2021.125902>](#)
- 1066 Cuesta, F., Tovar, C., Llambí, L.D., Gosling, W.D., Halloy, S., Carilla, J., Muriel, P., Meneses, R.I., Beck, S., Ulloa Ulloa, C.,
1067 Yager, K., Aguirre, N., Viñas, P., Jácome, J., Suárez-Duque, D., Buytaert, W., Pauli, H., 2020. Thermal niche traits
1068 of high alpine plant species and communities across the tropical Andes and their vulnerability to global warming. *J.*
1069 *Biogeogr.* 47, 408–420. <https://doi.org/10.1111/jbi.13759>
- 1070 Cuyckens, G.A.E., Christie, D.A., Domic, A.I., Malizia, L.R., Renison, D., 2016. Climate change and the distribution and
1071 conservation of the world's highest elevation woodlands in the South American Altiplano. *Glob. Planet. Change* 137,
1072 79–87. <https://doi.org/10.1016/j.gloplacha.2015.12.010>
- 1073 Cybis Elektronik, 2010. CDendro and CoRecorder [WWW Document]. URL <http://www.cybis.se/forfun/dendro/index.htm>

Formatted: Border: Top: (No border), Bottom: (No border), Left: (No border), Right: (No border), Between : (No border)

Formatted: Font color: Black

Formatted: Border: Top: (No border), Bottom: (No border), Left: (No border), Right: (No border), Between : (No border)

- 1074 D'Arrigo, R., Wilson, R., Liepert, B., Cherubini, P., 2008. On the 'Divergence Problem' in Northern Forests: A review of the
1075 tree-ring evidence and possible causes. *Glob. Planet. Change* 60, 289–305.
1076 <https://doi.org/10.1016/j.gloplacha.2007.03.004>
- 1077 D'Arrigo, R.D., Kaufmann, R.K., Davi, N., Jacoby, G.C., Laskowski, C., Myneni, R.B., Cherubini, P., 2004. Thresholds for
1078 warming-induced growth decline at elevational tree line in the Yukon Territory, Canada. *Glob. Biogeochem. Cycles*
1079 18. <https://doi.org/10.1029/2004GB002249>
- 1080 Devi, N.M., Kukarskih, V.V., Galimova, A.A., Mazepa, V.S., Grigoriev, A.A., 2020. Climate change evidence in tree growth
1081 and stand productivity at the upper treeline ecotone in the Polar Ural Mountains. *For. Ecosyst.* 7, 7.
1082 <https://doi.org/10.1186/s40663-020-0216-9>
- 1083 Duque, A., Peña, M.A., Cuesta, F., González-Caro, S., Kennedy, P., Phillips, O.L., Calderón-Loor, M., Blundo, C., Carilla, J.,
1084 Cayola, L., Farfán-Ríos, W., Fuentes, A., Grau, R., Homeier, J., Loza-Rivera, M.I., Malhi, Y., Malizia, A., Malizia,
1085 L., Martínez-Villa, J.A., Myers, J.A., Osinaga-Acosta, O., Peralvo, M., Pinto, E., Saatchi, S., Silman, M., Tello, J.S.,
1086 Terán-Valdez, A., Feeley, K.J., 2021. Mature Andean forests as globally important carbon sinks and future carbon
1087 refuges. *Nat. Commun.* 12, 2138. <https://doi.org/10.1038/s41467-021-22459-8>
- 1088 D'Arrigo, R., Jacoby, G., Free, M., Robock, A., 1999. Northern Hemisphere Temperature Variability for the Past Three
1089 Centuries: Tree-Ring and Model Estimates. *Clim. Change* 42, 663–675. <https://doi.org/10.1023/A:1005471918574>
- 1090 D'Arrigo, R., Wilson, R., Liepert, B., Cherubini, P., 2008. On the 'Divergence Problem' in Northern Forests: A review of the
1091 tree-ring evidence and possible causes. *Glob. Planet. Change* 60, 289–305.
1092 <https://doi.org/10.1016/j.gloplacha.2007.03.004>
- 1093 D'Arrigo, R.D., Kaufmann, R.K., Davi, N., Jacoby, G.C., Laskowski, C., Myneni, R.B., Cherubini, P., 2004. Thresholds for
1094 warming-induced growth decline at elevational tree line in the Yukon Territory, Canada. *Glob. Biogeochem. Cycles*
1095 18. <https://doi.org/10.1029/2004GB002249>
- 1096 Enfield, D.B., Mestas-Núñez, A.M., Mayer, D.A., Cid-Serrano, L., 1999. How ubiquitous is the dipole relationship in tropical
1097 Atlantic sea surface temperatures? *J. Geophys. Res. Oceans* 104, 7841–7848. <https://doi.org/10.1029/1998JC900109>
- 1098 Espinoza, J.-C., Arias, P.A., Moron, V., Junquas, C., Segura, H., Sierra-Pérez, J.P., Wongchuig, S., Condom, T., 2021. Recent
1099 Changes in the Atmospheric Circulation Patterns during the Dry-to-Wet Transition Season in South Tropical South
1100 America (1979–2020): Impacts on Precipitation and Fire Season. *J. Clim.* 34, 9025–9042.
1101 <https://doi.org/10.1175/JCLI-D-21-0303.1>
- 1102 Espinoza, J.C., Ronchail, J., Marengo, J.A., Segura, H., 2019. Contrasting North–South changes in Amazon wet-day and dry-
1103 day frequency and related atmospheric features (1981–2017). *Clim. Dyn.* 52, 5413–5430.
1104 <https://doi.org/10.1007/s00382-018-4462-2>
- 1105 Espinoza, J.C., Segura, H., Ronchail, J., Drapeau, G., Gutierrez-Cori, O., 2016. Evolution of wet-day and dry-day frequency
1106 in the western Amazon basin: Relationship with atmospheric circulation and impacts on vegetation. *Water Resour.*
1107 *Res.* 52, 8546–8560. <https://doi.org/10.1002/2016WR019305>
- 1108 Espinoza, T.E.B., Kessler, M., 2022. A monograph of the genus *Polylepis* (Rosaceae). *PhytoKeys* 203, 1–274.
1109 <https://doi.org/10.3897/phytokeys.203.83529>
- 1110 Fajardo, A., Gazol, A., Mayr, C., Camarero, J.J., 2019. Recent decadal drought reverts warming-triggered growth enhancement
1111 in contrasting climates in the southern Andes tree line. *J. Biogeogr.* 46, 1367–1379. <https://doi.org/10.1111/jbi.13580>
- 1112 Farfan-Rios, W., Feeley, K.J., Myers, J.A., Tello, S., Sallo-Bravo, J., Malhi, Y., Phillips, O.L., Baker, T.R., Nina-Quispe, A.,
1113 Garcia-Cabrera, K., 2025. Amazonian and Andean tree communities are not tracking current climate warming. *Proc.*
1114 *Natl. Acad. Sci.* 122, e2425619122.
- 1115 Feeley, K.J., Rehm, E.M., Machovina, B., 2012. perspective: The responses of tropical forest species to global climate change:
1116 acclimate, adapt, migrate, or go extinct? *Front. Biogeogr.* 4. <https://doi.org/10.21425/F5FBG12621>
- 1117 Feeley, K.J., Silman, M.R., Bush, M.B., Farfan, W., Cabrera, K.G., Malhi, Y., Meir, P., Revilla, N.S., Quisuypanqui, M.N.R.,
1118 Saatchi, S., 2011. Upslope migration of Andean trees. *J. Biogeogr.* 38, 783–791. <https://doi.org/10.1111/j.1365-2699.2010.02444.x>
- 1119 Ferrero, M.E., Villalba, R., De Membiela, M., Ripalta, A., Delgado, S., Paolini, L., 2013. Tree-growth responses across
1120 environmental gradients in subtropical Argentinean forests. *Plant Ecol.* 214, 1321–1334.
1121 <https://doi.org/10.1007/s11258-013-0254-2>
- 1122
1123 Finer, M., Mamani, N., 2023. Amazon Deforestation & Fire Hotspots 2022. *MAAP* 187, 2017–21.

Formatted: Border: Top: (No border), Bottom: (No border), Left: (No border), Right: (No border), Between : (No border)

Formatted: Font color: Black

Formatted: Border: Top: (No border), Bottom: (No border), Left: (No border), Right: (No border), Between : (No border)

- 1124 Flynn, H., Camarero, J.J., Sanmiguel-Valladolid, A., Rojas Heredia, F., Domínguez Aguilar, P., Revuelto, J., López-Moreno,
1125 J.I., 2025. A shift in circadian stem increment patterns in a Pyrenean alpine treeline precedes spring growth after snow
1126 melting. *Biogeosciences* 22, 1135–1147. <https://doi.org/10.5194/bg-22-1135-2025>
- 1127 Frank, D., Esper, J., Cook, E., 2006. On variance adjustments in tree-ring chronology development. *Tree Rings Archaeol.*
1128 *Climatol. Ecol. TRACE* 4, 56–66.
- 1129 Fritts, H.C., 1976. *Tree rings and Climate*. Academic Press, London.
- 1130 Fu, R., Yin, L., Li, W., Arias, P.A., Dickinson, R.E., Huang, L., Chakraborty, S., Fernandes, K., Liebmann, B., Fisher, R.,
1131 Myneni, R.B., 2013. Increased dry-season length over southern Amazonia in recent decades and its implication for
1132 future climate projection. *Proc. Natl. Acad. Sci.* 110, 18110–18115. <https://doi.org/10.1073/pnas.1302584110>
- 1133 Fuentes, A., 2005. Una introducción a la vegetación de la región de Madidi 32.
- 1134 Funk, C., Peterson, P., Landsfeld, M., Pedreros, D., Verdin, J., Shukla, S., Husak, G., Rowland, J., Harrison, L., Hoell, A.,
1135 2015. The climate hazards infrared precipitation with stations—a new environmental record for monitoring extremes.
1136 *Sci. Data* 2, 1–21.
- 1137 García-Núñez, C., Rada, F., Boero, C., González, J., Gallardo, M., Azócar, A., Liberman-Cruz, M., Hilal, M., Prado, F., 2004.
1138 Leaf Gas Exchange and Water Relations in *Polylepis tarapacana* at Extreme Altitudes in the Bolivian Andes.
1139 *Photosynthetica* 42, 133–138. <https://doi.org/10.1023/B:PHOT.0000040581.94641.ed>
- 1140 Garreaud, R., 1999. Multiscale Analysis of the Summertime Precipitation over the Central Andes.
- 1141 Garreaud, R.D., 2009. The Andes climate and weather. *Adv. Geosci.* 22, 3–11. <https://doi.org/10.5194/adgeo-22-3-2009>
- 1142 Good, P., Lowe, J.A., Collins, M., Moufouma-Okia, W., 2008. An objective tropical Atlantic sea surface temperature gradient
1143 index for studies of south Amazon dry-season climate variability and change. *Philos. Trans. R. Soc. B Biol. Sci.* 363,
1144 1761–1766. <https://doi.org/10.1098/rstb.2007.0024>
- 1145 Groenendijk, P., Babst, F., Trouet, V., Fan, Z.-X., Granato-Souza, D., Locosselli, G.M., Mokria, M., Panthi, S., Pumijumnong,
1146 N., Abiyu, A., Acuña-Soto, R., Adenky-Filho, E., Alfaro-Sánchez, R., Anholetto Junior, C.R., Aragão, J.R.V.,
1147 Assis-Pereira, G., Astudillo-Sánchez, C.C., Carolina Barbosa, A., Barreto, N. de O., Battipaglia, G., Beeckman, H.,
1148 Botosso, P.C., Bourland, N., Bräuning, A., Brienen, R., Brookhouse, M., Buajan, S., Buckley, B.M., Camarero, J.J.,
1149 Carrillo-Parra, A., Ceccantini, G., Centeno-Erguera, L.R., Cerano-Paredes, J., Cervantes-Martínez, R., Chanthorn,
1150 W., Chen, Y.-J., Cintra, B.B.L., Cornejo-Oviedo, E.H., Cortés-Cortés, O., Costa, C.M., Couralet, C., Crispin-
1151 DelaCruz, D.B., D'Arrigo, R., David, D.A., De Ridder, M., Del Valle, J.I., Díaz-Carrillo, O.A., Dobner Jr, M., Doucet,
1152 J.-L., Dünisch, O., Enquist, B.J., Esemann-Quadros, K., Esquivel-Arriaga, G., Fayolle, A., Fenilli, T.A.B., Ferrero,
1153 M.E., Fichtler, E., Finnegan, P.M., Fontana, C., Francisco, K.S., Fu, P.-L., Galvão, F., Gebrekirstos, A., Giraldo, J.A.,
1154 Gloor, E., Godoy-Veiga, M., Guerra, A., Haneca, K., Harley, G.L., Heinrich, I., Helle, G., Hernández-Díaz, J.C.,
1155 Hornink, B., Hubau, W., Inga, J.G., Islam, M., Jiang, Y., Kaib, M., Hassan Khamisi, Z., Koprowski, M., Layme, E.,
1156 Leffler, A.J., Ligot, G., Lisi, C.S., Loader, N.J., Lobo, F. de A., Longhi-Santos, T., Lopez, L., López-Hernández, M.I.,
1157 Lousada, J.L.P.C., Manzanedo, R.D., Marcon, A.K., Maxwell, J.T., Mendivelso, H.A., Mendoza-Villa, O.N.,
1158 Menezes, Í.R.N., Montóia, V.R., Moors, E., Moreno, M., Muñoz-Castro, M.A., Nabais, C., Nathalang, A., Ngoma, J.,
1159 Nogueira Jr., F. de C., Oliveira, J.M., Olmedo, G.M., Ortega-Rodríguez, D.R., Ortiz, C.E.R., Pagotto, M.A., Paredes-
1160 Villanueva, K., Pérez-De-Lis, G., Ponce Calderón, L.P., Portal-Cahuana, L.A., Pucha-Cofrep, D.A., Quadri, P.,
1161 Rahman, M., Ramírez, J.A., Requena-Rojas, E.J., Reyes-Flores, J., Ribeiro, A. de S., Robertson, I., Roig, F.A.,
1162 Roquette, J.G., Rubio-Camacho, E.A., Sánchez-Salguero, R., Sass-Klaassen, U., Schöngart, J., Scipioni, M.C.,
1163 Sheppard, P.R., Silva, L.C.R., Slotta, F., Soria-Díaz, L., Sousa, L.K.V.S., Speer, J.H., Therrell, M.D., Tisce-Otarola,
1164 G., Tomazello-Filho, M., Torbenson, M.C.A., Tor-Ngern, P., Touchan, R., Van Den Bulcke, J., Vázquez-Selem, L.,
1165 Velázquez-Pérez, A.H., Venegas-González, A., Villalba, R., Villanueva-Díaz, J., Vlam, M., Vourlitis, G., Wehenkel,
1166 C., Wils, T., Zavaleta, E.S., Zewdu, E.A., Zhang, Y.-J., Zhou, Z.-K., Zuidema, P.A., 2025. The importance of tropical
1167 tree-ring chronologies for global change research. *Quat. Sci. Rev.* 355, 109233.
1168 <https://doi.org/10.1016/j.quascirev.2025.109233>
- 1169 Harris, I., Osborn, T.J., Jones, P., Lister, D., 2020. Version 4 of the CRU TS monthly high-resolution gridded multivariate
1170 climate dataset. *Sci. Data* 7, 109. <https://doi.org/10.1038/s41597-020-0453-3>
- 1171 Haurwitz, M.W., Brier, G.W., 1981. A critique of the superposed epoch analysis method: its application to solar-weather
1172 relations. *Mon. Weather Rev.* 109, 2074–2079.

Formatted: Border: Top: (No border), Bottom: (No border),
Left: (No border), Right: (No border), Between : (No border)

Formatted: Border: Top: (No border), Bottom: (No border),
Left: (No border), Right: (No border), Between : (No border)

- 173 Hertel, D., Wesche, K., 2008. Tropical moist Polylepis stands at the treeline in East Bolivia: the effect of elevation on stand
174 microclimate, above- and below-ground structure, and regeneration. *Trees* 22, 303–315.
175 <https://doi.org/10.1007/s00468-007-0185-4>
- 176 Hoch, G., Körner, C., 2005. Growth, Demography and Carbon Relations of Polylepis Trees at the World's Highest Treeline.
177 *Funct. Ecol.* 19, 941–951.
- 178 Hock, R., Rasul, G., Adler, C., Caceres, B., Gruber, S., Hirabayashi, Y., Jackson, M., Käab, A., Kang, S., Kutuzov, S., Milner,
179 A., Molau, U., Morin, S., Orlove, B., Steltzer, H., Allen, S., Arenson, L., Banceerjee, S., Barr, I., Bórquez, R., Brown,
180 L., Cao, B., Carey, M., Cogley, G., Fischlin, A., A de Sherbinin, Eckert, N., Geertsema, M., Hagenstad, M., Honsberg,
181 M., Hood, E., Huss, M., E Jimenez Zamora, Kotlarski, S., Lefeuvre, P., J Ignacio López Moreno, Lundquist, J.,
182 Mcdowell, G., Mills, S., Mou, C., Nepal, S., Noetzi, J., Palazzi, E., Pepin, N., Rixen, C., Shahgedanova, M., S
183 McKenzie Skiles, Vincent, C., Viviroli, D., Gesa, A.W., P Yangjee Sherpa, Weyer, N., Wouters, B., Yasunari, T.,
184 You, Q., Zhang, Y., 2019. High Mountain Areas. STATI UNITI D'AMERICA.
- 185 Hoffmann, D., Weggenmann, D., 2013. Climate Change Induced Glacier Retreat and Risk Management: Glacial Lake Outburst
186 Floods (GLOFs) in the Apolobamba Mountain Range, Bolivia, in: Leal Filho, W. (Ed.), *Climate Change and Disaster*
187 *Risk Management, Climate Change Management.* Springer, Berlin, Heidelberg, pp. 71–87.
188 https://doi.org/10.1007/978-3-642-31110-9_5
- 189 Hua, Q., Turnbull, J.C., Santos, G.M., Rakowski, A.Z., Ancapichún, S., Pol-Holz, R.D., Hammer, S., Lehman, S.J., Levin, I.,
190 Miller, J.B., Palmer, J.G., Turney, C.S.M., 2022. ATMOSPHERIC RADIOCARBON FOR THE PERIOD 1950–
191 2019. *Radiocarbon* 64, 723–745. <https://doi.org/10.1017/RDC.2021.95>
- 192 [Huerta, A., Brönnimann, S., de Luis, M., Begueria, S., Serrano-Notivol, R., 2026. Enhancing daily precipitation
193 reconstruction: An improved version of the reddPrec R package. *Environ. Model. Softw.* 195, 106717.
194 <https://doi.org/10.1016/j.envsoft.2025.106717>](https://doi.org/10.1016/j.envsoft.2025.106717)
- 195 [Hunziker, S., Brönnimann, S., Calle, J., Moreno, J., Andrade, M., Ticona, L., Huerta, A., Lavado-Casimiro, W., 2018. Effects
196 of undetected data quality issues on climatological analyses. *Clim. Past* 14, 1–20. \[https://doi.org/10.5194/cp-14-1-
197 2018\]\(https://doi.org/10.5194/cp-14-1-2018\)](https://doi.org/10.5194/cp-14-1-2018)
- 198 Jacoby, G.C., D'Arrigo, R.D., 1995. Tree ring width and density evidence of climatic and potential forest change in Alaska.
199 *Glob. Biogeochem. Cycles* 9, 227–234. <https://doi.org/10.1029/95GB00321>
- 200 Jaramillo, A.D., 2015. Fotosíntesis en los Bosques a Mayor Elevación en el Planeta: Polylepis tarapacana en un Gradiente de
201 Elevación en los Andes de Arica y Parinacota, Chile.
- 202 Jomelli, V., Pavlova, I., Guin, O., Soliz-Gamboa, C., Contreras, A., Toivonen, J.M., Zetterberg, P., 2012. Analysis of the
203 Dendroclimatic Potential of Polylepis pepei, P. subsericans and P. rugulosa In the Tropical Andes (Peru-Bolivia).
204 *Tree-Ring Res.* 68, 91–103. <https://doi.org/10.3959/2011-10.1>
- 205 Junquas, C., Takahashi, K., Condom, T., Espinoza, J.-C., Chavez, S., Sicart, J.-E., Lebel, T., 2018. Understanding the influence
206 of orography on the precipitation diurnal cycle and the associated atmospheric processes in the central Andes. *Clim.*
207 *Dyn.* 50, 3995–4017. <https://doi.org/10.1007/s00382-017-3858-8>
- 208 Kessler, M., Toivonen, J.M., Sylvester, S.P., Kluge, J., Hertel, D., 2014. Elevational patterns of Polylepis tree height
209 (Rosaceae) in the high Andes of Peru: role of human impact and climatic conditions. *Front. Plant Sci.* 5.
210 <https://doi.org/10.3389/fpls.2014.00194>
- 211 Kolmogorov, A., 1933. Sulla determinazione empirica di una legge di distribuzione. *Giorn Dellinst Ital Degli Att* 4, 89–91.
- 212 [Kunsch, H.R., 1989. The Jackknife and the Bootstrap for General Stationary Observations. *Ann. Stat.* 17, 1217–1241.
213 <https://doi.org/10.1214/aos/1176347265>](https://doi.org/10.1214/aos/1176347265)
- 214 Körner, C., 2012. Definitions and conventions, in: Körner, C. (Ed.), *Alpine Treelines: Functional Ecology of the Global High*
215 *Elevation Tree Limits.* Springer, Basel, pp. 11–19. https://doi.org/10.1007/978-3-0348-0396-0_2
- 216 Körner, C., Hoch, G., 2023. Not every high-latitude or high-elevation forest edge is a treeline. *J. Biogeogr.* 50, 838–845.
217 <https://doi.org/10.1111/jbi.14593>
- 218 Locosselli, G.M., Brien, R.J.W., Leite, M. de S., Gloor, M., Krottenthaler, S., Oliveira, A.A. de, Barichivich, J., Anhof, D.,
219 Ceccantini, G., Schöngart, J., Buckenridge, M., 2020. Global tree-ring analysis reveals rapid decrease in tropical tree
220 longevity with temperature. *Proc. Natl. Acad. Sci.* 117, 33358–33364. <https://doi.org/10.1073/pnas.2003873117>

Formatted: Border: Top: (No border), Bottom: (No border),
Left: (No border), Right: (No border), Between : (No border)

Formatted: Border: Top: (No border), Bottom: (No border),
Left: (No border), Right: (No border), Between : (No border)

- 1221 López, V.L., Huertas Herrera, A., Rosas, Y.M., Cellini, J.M., 2022. Optimal environmental drivers of high-mountains forest:
1222 Polylepis tarapacana cover evaluation in their southernmost distribution range of the Andes. *Trees For. People* 9,
1223 100321. <https://doi.org/10.1016/j.tfp.2022.100321>
- 1224 MacDonald, G. m. Kremenetski, K. v. Beilman, D. w. 2007. Climate change and the northern Russian treeline zone. *Philos.*
1225 *Trans. R. Soc. B Biol. Sci.* 363, 2283–2299. <https://doi.org/10.1098/rstb.2007.2200>
- 1226 Macek, P., Macková, J., de Bello, F., 2009. Morphological and ecophysiological traits shaping altitudinal distribution of three
1227 Polylepis treeline species in the dry tropical Andes. *Acta Oecologica* 35, 778–785.
1228 <https://doi.org/10.1016/j.actao.2009.08.013>
- 1229 Macía, M.J., 2008. Woody plants diversity, floristic composition and land use history in the Amazonian rain forests of Madidi
1230 National Park, Bolivia. *Biodivers. Conserv.* 17, 2671–2690. <https://doi.org/10.1007/s10531-008-9348-x>
- 1231 Malhi, Y., Roberts, J.T., Betts, R.A., Killeen, T.J., Li, W., Nobre, C.A., 2008. Climate Change, Deforestation, and the Fate of
1232 the Amazon. *Science* 319, 169–172.
- 1233 Malizia, A., Blundo, C., Carilla, J., Acosta, O.O., Cuesta, F., Duque, A., Aguirre, N., Aguirre, Z., Ataroff, M., Baez, S.,
1234 Calderón-Loor, M., Cayola, L., Cayuela, L., Ceballos, S., Cedillo, H., Ríos, W.F., Feeley, K.J., Fuentes, A.F., Álvarez,
1235 L.E.G., Grau, R., Homeier, J., Jadan, O., Llambi, L.D., Rivera, M.I.L., Macía, M.J., Malhi, Y., Malizia, L., Peralvo,
1236 M., Pinto, E., Tello, S., Silman, M., Young, K.R., 2020. Elevation and latitude drives structure and tree species
1237 composition in Andean forests: Results from a large-scale plot network. *PLOS ONE* 15, e0231553.
1238 <https://doi.org/10.1371/journal.pone.0231553>
- 1239 Marengo, J.A., Tomasella, J., Alves, L.M., Soares, W.R., Rodriguez, D.A., 2011. The drought of 2010 in the context of
1240 historical droughts in the Amazon region. *Geophys. Res. Lett.* 38. <https://doi.org/10.1029/2011GL047436>
- 1241 Meko, D.M., Touchan, R., Anchukaitis, K.J., 2011. Seacorr: A MATLAB program for identifying the seasonal climate signal
1242 in an annual tree-ring time series. *Comput. Geosci.* 37, 1234–1241. <https://doi.org/10.1016/j.cageo.2011.01.013>
- 1243 Melvin, T., 2004. Historical growth rates and changing climatic sensitivity of boreal conifers.
- 1244 Montaña-Centellas, F., Fuentes, A.F., Cayola, L., Macía, M.J., Arellano, G., Loza, M.I., Nieto-Ariza, B., Tello, J.S., 2024.
1245 Elevational range sizes of woody plants increase with climate variability in the Tropical Andes. *J. Biogeogr.* 51, 814–
1246 826. <https://doi.org/10.1111/jbi.14783>
- 1247 Morales, M.S., Crispin-DelaCruz, D.B., Álvarez, C., Christie, D.A., Ferrero, M.E., Andreu-Hayles, L., Villalba, R., Guerra,
1248 A., Ticse-Otarola, G., Rodríguez-Ramírez, E.C., LLocella-Martínez, R., Sanchez-Ferrer, J., Requena-Rojas, E.J.,
1249 2023. Drought increase since the mid-20th century in the northern South American Altiplano revealed by a 389-year
1250 precipitation record. *Clim. Past* 19, 457–476. <https://doi.org/10.5194/cp-19-457-2023>
- 1251 Morales, M.S., Villalba, R., Grau, H.R., Paolini, L., 2004. Rainfall-Controlled Tree Growth in High-Elevation Subtropical
1252 Treelines. *Ecology* 85, 3080–3089. <https://doi.org/10.1890/04-0139>
- 1253 Muller, M.R., 2017. Protected areas and their relationship with food security in a context of climate change: an overview from
1254 Bolivia, Brazil and Peru. *Prot. AREAS*.
- 1255 Nagy, L., Eller, C.B., Mercado, L.M., Cuesta, F.X., Llambí, L.D., Buscardo, E., Aragão, L.E.O.C., García-Núñez, C., Oliveira,
1256 R.S., Barbosa, M., Ceballos, S.J., Calderón-Loor, M., Fernandes, G.W., Aráoz, E., Muñoz, A.M.Q., Rozzi, R.,
1257 Aguirre, F., Álvarez-Dávila, E., Salinas, N., Sitch, S., 2023. South American mountain ecosystems and global change
1258 – a case study for integrating theory and field observations for land surface modelling and ecosystem management.
1259 *Plant Ecol. Divers.* 16, 1–27. <https://doi.org/10.1080/17550874.2023.2196966>
- 1260 Navarro, G., Arrázola, S., Balderrama, J.A., Ferreira, W., De la Barra, N., Antezana, C., Gómez, I., Mercado, M., 2010.
1261 Diagnóstico del estado de conservación y caracterización de los bosques de Polylepis en Bolivia y su avifauna
1262 Conservation state analysis and characterization of the Bolivian Polylepis forests and their avifauna. *Rev. Bolív. Ecol.*
1263 *Conserv. Ambient.* 28, 1–35.
- 1264 Oelkers, R.C., Andreu-Hayles, L., D'Arrigo, R., Pacheco-Solana, A., Rodriguez-Caton, M., Fuentes, A., Santos, G.M.,
1265 Tejedor, E., Ferrero, M.E., Maldonado, C., 2023. Recent growth increase in endemic Juglans boliviana from the
1266 tropical Andes. *Dendrochronologia* 79, 126090. <https://doi.org/10.1016/j.dendro.2023.126090>
- 1267 Paegle, J.N., Mo, K.C., 2002. Linkages between Summer Rainfall Variability over South America and Sea Surface
1268 Temperature Anomalies.
- 1269 Paulsen, J., Weber, U. M., and Körner, Ch., 2000. Tree Growth near Treeline: Abrupt or Gradual Reduction with Altitude?
1270 *Arct. Antarct. Alp. Res.* 32, 14–20. <https://doi.org/10.1080/15230430.2000.12003334>

Formatted: Border: Top: (No border), Bottom: (No border),
Left: (No border), Right: (No border), Between : (No border)

Formatted: Border: Top: (No border), Bottom: (No border),
Left: (No border), Right: (No border), Between : (No border)

- 1271 Pettitt, A.N., 1979. A Non-Parametric Approach to the Change-Point Problem. *J. R. Stat. Soc. Ser. C Appl. Stat.* 28, 126–135.
1272 <https://doi.org/10.2307/2346729>
- 1273 Politis, D.N., Romano, J.P., 1994. The Stationary Bootstrap. *J. Am. Stat. Assoc.* 89, 1303–1313.
1274 <https://doi.org/10.1080/01621459.1994.10476870>
- 1275 Quesada-Román, A., Ballesteros-Cánovas, J.A., St. George, S., Stoffel, M., 2022. Tropical and subtropical dendrochronology:
1276 Approaches, applications, and prospects. *Ecol. Indic.* 144, 109506. <https://doi.org/10.1016/j.ecolind.2022.109506>
- 1277 Rao, M.P., Cook, E.R., Cook, B.I., Anchukaitis, K.J., D'Arrigo, R.D., Krusic, P.J., LeGrande, A.N., 2019. A double bootstrap
1278 approach to Superposed Epoch Analysis to evaluate response uncertainty. *Dendrochronologia* 55, 119–124.
1279 <https://doi.org/10.1016/j.dendro.2019.05.001>
- 1280 Rasmusson, E.M., Carpenter, T.H., 1982. Variations in tropical sea surface temperature and surface wind fields associated
1281 with the Southern Oscillation/El Niño. *Mon. Weather Rev.* 110, 354–384.
- 1282 Rehm, E.M., Feeley, K.J., 2013. Forest patches and the upward migration of timberline in the southern Peruvian Andes. *For.*
1283 *Ecol. Manag.* 305, 204–211. <https://doi.org/10.1016/j.foreco.2013.05.041>
- 1284 Requena-Rojas, E.J., Amoroso, M.M., Ticse-Otarola, G., Crispin-Delacruz, D.B., 2021. Assessing Dendrochronological
1285 Potential of *Escallonia myrtilloides* in the High Andes of Peru. *Tree-Ring Res.* 77, 41–52.
1286 <https://doi.org/10.3959/TRR2019-8>
- 1287 Requena-Rojas, E.J., Crispin-DelaCruz, D.B., Ticse-Otarola, G., Quispe-Melgar, H.R., Inga Guillen, J.G., Camel Paucar, V.,
1288 Guerra, A., Ames-Martinez, F.N., Morales, M., 2020. Temporal Growth Variation in High-Elevation Forests: Case
1289 Study of *Polylepis* Forests in Central Andes, in: Pompa-García, M., Camarero, J.J. (Eds.), *Latin American*
1290 *Dendroecology: Combining Tree-Ring Sciences and Ecology in a Megadiverse Territory*. Springer International
1291 Publishing, Cham, pp. 263–279. https://doi.org/10.1007/978-3-030-36930-9_12
- 1292 Rodriguez-Caton, M., Andreu-Hayles, L., Morales, M.S., Daux, V., Christie, D.A., Coopman, R.E., Alvarez, C., Rao, M.P.,
1293 Aliste, D., Flores, F., Villalba, R., 2021. Different climate sensitivity for radial growth, but uniform for tree-ring
1294 stable isotopes along an aridity gradient in *Polylepis tarapacana*, the world's highest elevation tree species. *Tree*
1295 *Physiol.* 41, 1353–1371. <https://doi.org/10.1093/treephys/tpab021>
- 1296 Rodriguez-Caton, M., Morales, M.S., Rao, M.P., Nixon, T., Vuille, M., Rivera, J.A., Oelkers, R., Christie, D.A., Varuolo-
1297 Clarke, A.M., Ferrero, M.E., Magney, T., Daux, V., Villalba, R., Andreu-Hayles, L., 2024. A 300-year tree-ring
1298 $\delta^{18}\text{O}$ -based precipitation reconstruction for the South American Altiplano highlights decadal hydroclimate
1299 teleconnections. *Commun. Earth Environ.* 5, 1–13. <https://doi.org/10.1038/s43247-024-01385-9>
- 1300 Rodriguez-Caton, M., Andreu-Hayles, L., Daux, V., Vuille, M., Varuolo-Clarke, A.M., Oelkers, R., Christie, D.A., D'Arrigo,
1301 R., Morales, M.S., Palat Rao, M., Srur, A.M., Vimeux, F., Villalba, R., 2022. Hydroclimate and ENSO Variability
1302 Recorded by Oxygen Isotopes From Tree Rings in the South American Altiplano. *Geophys. Res. Lett.* 49,
1303 <https://doi.org/10.1029/2021GL095883>
- 1304 Roig, F., Fernández, M., Gareca León, E., Altamirano, S., Monge, S., 2001. ESTUDIOS DENDROCRONOLÓGICOS EN
1305 LOS AMBIENTES HÚMEDOS DE LA PUNA BOLIVIANA DENDROCHRONOLOGICAL STUDIES IN THE
1306 HUMID PUNA ENVIRONMENTS OF BOLIVIA. *Rev Bol Ecol* 9.
- 1307 Rolland, C., Petitcolas, V., Michalet, R., 1998. Changes in radial tree growth for *Picea abies*, *Larix decidua*, *Pinus cembra* and
1308 *Pinus uncinata* near the alpine timberline since 1750. *Trees* 13, 40–53. <https://doi.org/10.1007/PL00009736>
- 1309 Romatschke, U., Houze, R.A., 2010. Extreme Summer Convection in South America. <https://doi.org/10.1175/2010JCLI3465.1>
- 1310 Ronchail, J., Espinoza, J.C., Drapeau, G., Sabot, M., Cochonneau, G., Schor, T., 2018. The flood recession period in Western
1311 Amazonia and its variability during the 1985–2015 period. *J. Hydrol. Reg. Stud.* 15, 16–30.
1312 <https://doi.org/10.1016/j.ejrh.2017.11.008>
- 1313 Ropelewski, C.F., Halpert, M.S., 1987. Global and Regional Scale Precipitation Patterns Associated with the El Niño/Southern
1314 Oscillation.
- 1315 Rosales, A.G., Junquas, C., Rocha, R.P. da, Condom, T., Espinoza, J.-C., 2022. Valley–Mountain Circulation Associated with
1316 the Diurnal Cycle of Precipitation in the Tropical Andes (Santa River Basin, Peru). *Atmosphere* 13,
1317 <https://doi.org/10.3390/atmos13020344>
- 1318 Schulman, E., 1956. *Dendroclimatic Changes in Semiarid America*. University of Arizona Press, Tucson, p. 142.

Formatted: Border: Top: (No border), Bottom: (No border),
Left: (No border), Right: (No border), Between : (No border)

Formatted: Border: Top: (No border), Bottom: (No border),
Left: (No border), Right: (No border), Between : (No border)

1319 Segura, H., Espinoza, J.C., Junquas, C., Lebel, T., Vuille, M., Condom, T., 2022. Extreme austral winter precipitation events
1320 over the South-American Altiplano: regional atmospheric features. *Clim. Dyn.* 59, 3069–3086.
1321 <https://doi.org/10.1007/s00382-022-06240-1>

1322 Sierra, J.P., Junquas, C., Espinoza, J.C., Segura, H., Condom, T., Andrade, M., Molina-Carpio, J., Ticona, L., Mardoñez, V.,
1323 Blacutt, L., Polcher, J., Rabatel, A., Sicart, J.E., 2022. Deforestation impacts on Amazon-Andes hydroclimatic
1324 connectivity. *Clim. Dyn.* 58, 2609–2636. <https://doi.org/10.1007/s00382-021-06025-y>

1325 Simpson, B.B., 1979. A revision of the genus *Polylepis* (Rosaceae: Sanguisorbeae). *Smithson. Contrib. Bot.*
1326 Smirnov, N., 1948. Table for estimating the goodness of fit of empirical distributions. *Ann. Math. Stat.* 19, 279–281.

1327 Srur, A.M., Villalba, R., Rodríguez-Catón, M., Amoroso, M.M., Marcotti, E., 2018. Climate and *Nothofagus pumilio*
1328 Establishment at Upper Treelines in the Patagonian Andes. *Front. Earth Sci.* 6.
1329 <https://doi.org/10.3389/feart.2018.00057>

1330 Srur, A.M., Villalba, Ricardo, Rodríguez-Catón, Milagros, Amoroso, Mariano M., and Marcotti, E., 2016. Establishment of
1331 *Nothofagus pumilio* at Upper Treelines Across a Precipitation Gradient in the Northern Patagonian Andes. *Arct.*
1332 *Antarct. Alp. Res.* 48, 755–766. <https://doi.org/10.1657/AAAR0016-015>

1333 Stokes, M.A., Smiley, T.L., 1968. An introduction to tree-ring dating. University of Chicago Press, Chicago, Illinois.

1334 Thompson, L.G., Mosley-Thompson, E., Brecher, H., Davis, M., León, B., Les, D., Lin, P.-N., Mashiotta, T., Mountain, K.,
1335 2006. Abrupt tropical climate change: Past and present. *Proc. Natl. Acad. Sci.* 103, 10536–10543.
1336 <https://doi.org/10.1073/pnas.0603900103>

1337 Tovar, C., Carril, A.F., Gutiérrez, A.G., Ahrends, A., Fita, L., Zaninelli, P., Flombaum, P., Abarzúa, A.M., Alarcón, D.,
1338 Aschero, V., Báez, S., Barros, A., Carilla, J., Ferrero, M.E., Flantua, S.G.A., González, P., Menéndez, C.G., Pérez-
1339 Escobar, O.A., Pauchard, A., Ruscica, R.C., Särkinen, T., Sörensson, A.A., Srur, A., Villalba, R., Hollingsworth,
1340 P.M., 2022. Understanding climate change impacts on biome and plant distributions in the Andes: Challenges and
1341 opportunities. *J. Biogeogr.* 49, 1420–1442. <https://doi.org/10.1111/jbi.14389>

1342 Vera, C., Higgins, W., Amador, J., Ambrizzi, T., Garreaud, R., Gochis, D., Gutzler, D., Lettenmaier, D., Marengo, J., Mechoso,
1343 C.R., Noguez-Paegle, J., Silva Dias, P.L., Zhang, C., 2006. Toward a Unified View of the American Monsoon
1344 Systems. *J. Clim.* 19, 4977–5000. <https://doi.org/10.1175/JCLI3896.1>

1345 Virtanen, P., Gommers, R., Oliphant, T.E., Haberland, M., Reddy, T., Cournapeau, D., Burovski, E., Peterson, P., Weckesser,
1346 W., Bright, J., 2020. SciPy 1.0: fundamental algorithms for scientific computing in Python. *Nat. Methods* 17, 261–
1347 272.

1348 von Arx, G., Crivellaro, A., Prendin, A.L., Čufar, K., Carrer, M., 2016. Quantitative Wood Anatomy—Practical Guidelines.
1349 *Front. Plant Sci.* 7.

1350 Vuille, M., Bradley, R.S., Keimig, F., 2000. Interannual climate variability in the Central Andes and its relation to tropical
1351 Pacific and Atlantic forcing. *J. Geophys. Res. Atmospheres* 105, 12447–12460.
1352 <https://doi.org/10.1029/2000JD900134>

1353 Waskom, M.L., 2021. seaborn: statistical data visualization. *J. Open Source Softw.* 6, 3021.
1354 <https://doi.org/10.21105/joss.03021>

1355 Wigley, T.M.L., Briffa, K.R., Jones, P.D., 1984. On the Average Value of Correlated Time Series, with Applications in
1356 Dendroclimatology and Hydrometeorology. *J. Appl. Meteorol. Climatol.* 23, 201–213. [https://doi.org/10.1175/1520-0450\(1984\)023<0201:OTAVOC>2.0.CO;2](https://doi.org/10.1175/1520-0450(1984)023<0201:OTAVOC>2.0.CO;2)

1357 [https://doi.org/10.1175/1520-0450\(1984\)023<0201:OTAVOC>2.0.CO;2](https://doi.org/10.1175/1520-0450(1984)023<0201:OTAVOC>2.0.CO;2)

1358 [Wilke, C.O., Wilke, M.C.O., 2022. Package 'ggridges.' Ridgeline Plots "ggplot2".](https://doi.org/10.1175/1520-0450(1984)023<0201:OTAVOC>2.0.CO;2)

1359 Wilmking, M., D'Arrigo, R., Jacoby, G.C., Juday, G.P., 2005. Increased temperature sensitivity and divergent growth trends
1360 in circumpolar boreal forests. *Geophys. Res. Lett.* 32. <https://doi.org/10.1029/2005GL023331>

1361 Wolter, K., Timlin, M.S., 2011. El Niño/Southern Oscillation behaviour since 1871 as diagnosed in an extended multivariate
1362 ENSO index (MEI.ext). *Int. J. Climatol.* 31, 1074–1087. <https://doi.org/10.1002/joc.2336>

1363 Yoon, J., Zeng, N., 2010. An Atlantic influence on Amazon rainfall. *Clim. Dyn.* 34, 249–264. <https://doi.org/10.1007/s00382-009-0551-6>

1364 Young, K.R., León, B., 2006. Tree-line changes along the Andes: implications of spatial patterns and dynamics. *Philos. Trans.*
1365 *R. Soc. B Biol. Sci.* 362, 263–272. <https://doi.org/10.1098/rstb.2006.1986>

1366 Zang, C., Biondi, F., 2015. treeclim: an R package for the numerical calibration of proxy-climate relationships. *Ecography* 38,
1367 431–436. <https://doi.org/10.1111/ecog.01335>

Formatted: Border: Top: (No border), Bottom: (No border),
Left: (No border), Right: (No border), Between : (No border)

Formatted: Border: Top: (No border), Bottom: (No border),
Left: (No border), Right: (No border), Between : (No border)

- 1369 Zanin, P.R., Satyamurty, P., 2020. Hydrological processes interconnecting the two largest watersheds of South America from
1370 multi-decadal to inter-annual time scales: A critical review. *Int. J. Climatol.* 40, 4006–4038.
1371 <https://doi.org/10.1002/joc.6442>
- 1372 Zapata, F., 2013. A multilocus phylogenetic analysis of Escallonia (Escalloniaceae): Diversification in montane South
1373 America. *Am. J. Bot.* 100, 526–545. <https://doi.org/10.3732/ajb.1200297>
- 1374
- 1375
- 1376 [Zelazowski, P., Jozefowicz, S., Feeley, K.J., Malhi, Y., 2023. Establishing the Position and Drivers of the Eastern Andean](#)
1377 [Treeline with Automated Transect Sampling. *Remote Sens.* 15, 2679. <https://doi.org/10.3390/rs15102679>](#)
- 1378

Formatted: Border: Top: (No border), Bottom: (No border),
Left: (No border), Right: (No border), Between : (No border)

Formatted: Border: Top: (No border), Bottom: (No border),
Left: (No border), Right: (No border), Between : (No border)